European Journal of Medicinal Chemistry 235 (2022) 114240

Contents lists available at ScienceDirect

European Journal of Medicinal Chemistry

journal homepage: http://www.elsevier.com/locate/ejmech

A chemoinformatics search for peroxisome proliferator-activated receptors ligands revealed a new pan-agonist able to reduce lipid accumulation and improve insulin sensitivity

Sabina Sblano [a, 1], Carmen Cerchia [b, 1], Antonio Laghezza [a], Luca Piemontese [a], Leonardo Brunetti [a], Rosalba Leuci [a], Federica Gilardi [c, d], Aurelien Thomas [c, d], Massimo Genovese [e], Alice Santi [e], Paolo Tortorella [a], Paolo Paoli [e], Antonio Lavecchia [b, **], Fulvio Loiodice [a, *]

[a] Dipartimento Farmacia-Scienze del Farmaco, Università degli Studi di Bari "Aldo Moro", Via Orabona 4, 70125, Bari, Italy
[b] Dipartimento di Farmacia, "Drug Discovery" Laboratory, Università degli Studi di Napoli "Federico II", Via D. Montesano 49, 80131, Napoli, Italy
[c] Faculty Unit of Toxicology, University Center of Legal Medicine, Lausanne University Hospital and University of Lausanne, Chemin de la Vulliette 4, CH-1000 Lausanne 25, Switzerland
[d] Unit of Forensic Toxicology and Chemistry, University Center of Legal Medicine, Lausanne University Hospital and University of Lausanne, Geneva University Hospital and University of Geneva, Lausanne, Geneva, Switzerland
[e] Dipartimento di Scienze Biomediche Sperimentali e Cliniche, Sezione di Scienze Biochimiche, Università degli Studi di Firenze, Viale Morgagni 50, 50134, Firenze, Italy

ARTICLE INFO

Article history:
Received 21 December 2021
Received in revised form
3 February 2022
Accepted 24 February 2022
Available online 16 March 2022

Keywords:
Chemoinformatics search
PPAR pan-agonist
Docking experiments
Glucose uptake

ABSTRACT

The peroxisome proliferator-activated receptors (PPARs) are nuclear receptors involved in the regulation of the metabolic homeostasis and therefore represent valuable therapeutic targets for the treatment of metabolic diseases. The development of more balanced drugs interacting with PPARs, devoid of the side-effects showed by the currently marketed PPARγ full agonists, is considered the major challenge for the pharmaceutical companies. Here we present a chemoinformatics search approach for new ligands that let us identify a novel PPAR pan-agonist with a very attractive activity profile being able to reduce lipid accumulation and improve insulin sensitivity. This compound represents, therefore, the potential lead of a new class of drugs for treatment of dyslipidemic type 2 diabetes.

1. Introduction

Peroxisome Proliferator-Activated Receptors (PPARs) control important metabolic functions in the body, mainly implicated in lipid and glucose homeostasis, insulin sensitivity, and energetic metabolism. The PPARs family comprises three different subtypes: α, β/δ and γ, whose expression and actions differ according to subtype, organ and tissue cell type [1].

PPARα is expressed in tissues with a high rate of fatty acid oxidation, such as skeletal muscle, liver, heart, kidney and brown adipose tissue, and modulates lipid metabolism and inflammation [2]. PPARγ is mainly expressed in adipose tissue, where it induces lipogenesis and fat storage, and in skeletal muscle, where it improves insulin sensitivity [3]. PPARδ, the less understood PPAR subtype, is more ubiquitously expressed; it is involved in metabolic disorders, inflammation, and angiogenesis [4].

The three PPARs subtypes share the same structure comprising of a ligand binding domain and a DNA-binding domain; in particular, the first interacts with different ligands, while the second one has a modulatory role [5]. Following interaction with agonists, PPARs are translocated to the nucleus, where they heterodimerize

Abbreviations: PPAR, peroxisome proliferator-activated receptor; TZDs, thiazolidinediones; SPPARM, selective peroxisome proliferator-activated receptor modulator; HMGCS2, hydroxymethylglutaryl-CoA synthase 2; FGF21, fibroblast growth factor 21; PDK4, pyruvate dehydrogenase kinase 4; FABP1, fatty acid binding protein 1; CPT1a, carnitine palmitoyl-transferase; ABCA1, ATP-binding cassette transporter A1; GLUT4, glucose transporter type 4.

** Corresponding author. .
* Corresponding author. .
E-mail addresses: antonio.lavecchia@unina.it (A. Lavecchia), fulvio.loiodice@uniba.it (F. Loiodice).

[1] S. Sblano and C. Cerchia contributed equally to this work.

https://doi.org/10.1016/j.ejmech.2022.114240
0223-5234/

with the retinoid X receptor (RXR). Then, this complex binds to peroxisome proliferator hormone response elements (PPREs) and regulates the expression of target genes [6]. Over the years, PPARs became a focus of interest due to their important role in the control of lipid and glucose homeostasis. These receptors are valuable targets for the treatment of metabolic syndrome, a group of risk factors for cardiovascular disease and type 2 diabetes mellitus (T2DM).

PPARα or PPARγ agonist drugs, such as fibrates or thiazolidinediones (TZDs), have been widely employed for lipid and glycemic control [7]. On the other hand, no PPARδ agonists have been approved for clinical use [8]. Safety-related issues with fibrates [9] prompted the development of PPARα agonists with improved clinical efficacy, such as Pemafibrate, endowed with superior benefit-risk balance compared to conventional fibrates [10]. TZDs use has been limited, or they have been withdrawn from the market in the United States, Europe and other countries [11], due to unwanted adverse effects, such as fluid retention, congestive heart failure (CHF) and adipogenic weight gain [7].

To overcome these issues, the concept of selective PPAR modulators (SPPARMs) with a superior balance of efficacy and safety has been proposed [12]. SPPARMs are able to induce distinct agonistic and antagonistic responses depending on the cellular context and specific transcriptional signatures.

Research efforts have been ultimately directed toward the design of new molecules beneficially altering carbohydrate and lipid metabolism in a coordinated manner. In fact, the development of PPARα/γ dual agonists or PPARα/γ/δ pan-agonists, acting on all three subtypes, has been considered a very attractive option for the development of hypolipidemic and antidiabetic drugs [13–16].

Besides dyslipidemia and T2DM, PPARs also have profound implications on other facets of metabolic syndrome, like diabetic complications, non-alcoholic fatty liver disease (NAFLD), as well as non-metabolic disorders, including neurodegenerative diseases, cancer, and inflammatory diseases. For instance, the dual PPARα/γ agonist Saroglitazar (Fig. 1) has been granted marketing authorization in India for the treatment of diabetic dyslipidemia not controlled with statins [17]. Lanifibranor, a well-balanced PPARα/γ/δ pan-agonist with an excellent safety profile [18], is currently in Phase II for NAFLD and T2DM. Chiglitazar, another PPARα/γ/δ pan-agonist, recently completed phase III clinical trials in China; the overall results showed that Chiglitazar was generally well tolerated in patients with T2DM, even the elderly ones [19].

In the search for new PPAR ligands with these properties, we recently identified, through structure-based virtual screening, a set of small molecules acting as PPAR ligands and exhibiting EC_{50} in the low micromolar range. In the present work, we employed one of these compounds reported in a previous paper [20], namely compound AL26 (therein termed **13**), which showed an interesting PPARα/γ dual agonism in transactivation assays, as a starting point to search for novel structural analogues, possibly endowed with α/γ dual- or even α/γ/δ pan-PPAR activity. A chemoinformatics search (schematized in Fig. S2, Supporting Information) was performed against the NCI Open Database, resulting in the selection of 16 compounds. Among them, three were identified as actives, through the use of PPAR-Gal4 transactivation assay (Table 1). PPAR subtype selectivity studies identified two dual targeting PPARα/γ agents plus a novel PPARα/γ/δ pan-agonist, with a moderate and balanced activation profile (AL26-18). The activity of AL26-18 prompted us to design and synthesize a novel series of derivatives (Table 2). Notably, two specific PPARα agonists with sub-micromolar potency, compounds **17** and **18**, emerged from this series. In addition, we prepared the two enantiomers of AL26-18 ((*R*)-**1** and (*S*)-**1**) and tested them in transactivation assay. Interestingly, only the *R* enantiomer turned out to be active. Docking experiments showed that (*R*)-**1** and (*S*)-**1** adopt very different binding modes in the three PPAR subtypes, and also provided insights into the structure-activity relationships (SARs) for the other derivatives. To investigate further the biological properties of (*R*)-**1**, we next assessed its activity on steatotic HepaRG cells and demonstrated its ability to reduce lipid accumulation. To explain the mechanisms underlying such improvement of hepatosteatosis, gene expression experiments on HepaRG cells were performed and the data obtained were compared with those obtained from reference compounds fenofibrate and rosiglitazone. The results showed an enhanced ability of (*R*)-**1** to induce the expression of several PPAR target genes

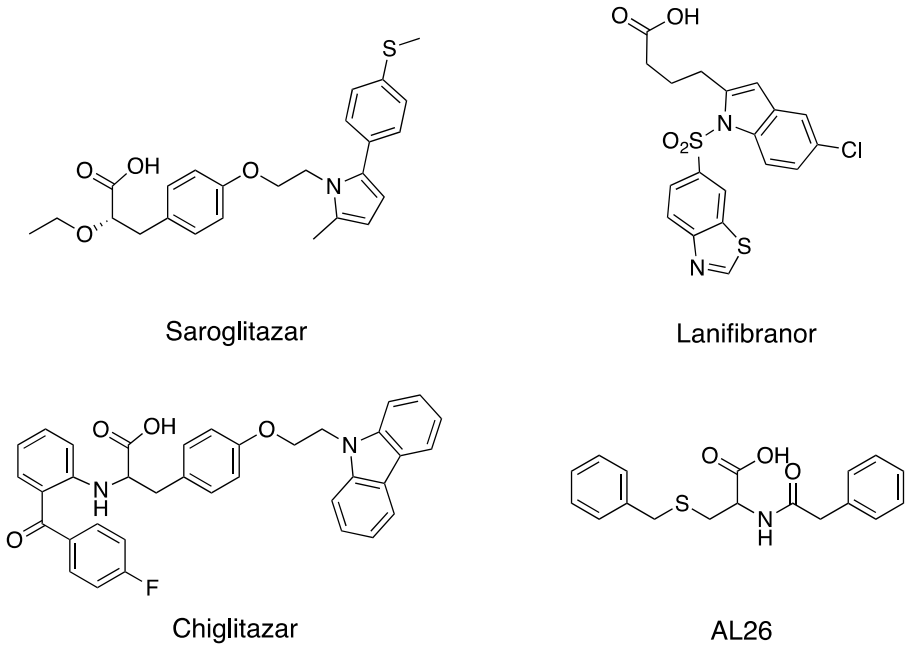

Fig. 1. Chemical structures of representative PPARα/γ dual- or α/γ/δ pan-agonists.

Table 1
Biological activities of selected compounds on PPARs.

Cpd	Structure	PPARα		PPARγ		PPARδ	
		EC_{50} (μM)	E_{max} (%)	EC_{50} (μM)	E_{max} (%)	EC_{50} (μM)	E_{max} (%)
AL26	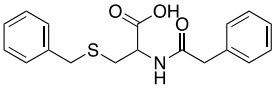	2.55 ± 0.35	148 ± 22	10.9 ± 2.4	16 ± 7	i.a.	i.a.
AL26-7	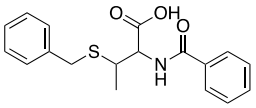	9.1 ± 1.2	48 ± 4	6.7 ± 1.6	33 ± 5	i.a.	i.a.
AL26-11	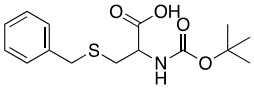	1.45 ± 0.49	118 ± 9	25.7 ± 1.3	22 ± 1	i.a.	i.a.
AL26-18	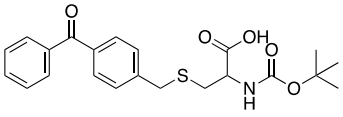	1.6 ± 0.7	83 ± 1	10.3 ± 0.6	15 ± 2	37.1 ± 2.1	59 ± 3
Wy-14,643		1.56 ± 0.3	100 ± 10	i.a.	i.a.	i.a.	i.a.
Rosiglitazone		i.a.	i.a.	0.04 ± 0.02	100 ± 9	i.a.	i.a.
L-165,045		i.a.	i.a.	i.a.	i.a.	0.021 ± 0.04	100 ± 4

i.a.: inactive at tested concentrations.

Table 2
Biological activities of novel analogues of AL26-18 on PPARs.

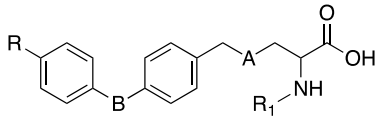

					PPARα		PPARγ		PPARβ/δ	
Cpd	R	B	A	R_1	EC_{50} (μM)	E_{max} (%)	EC_{50} (μM)	E_{max} (%)	EC_{50} (μM)	E_{max} (%)
1 (AL26-18)	H	CO	S	BOC	1.6 ± 0.7	83 ± 1	10.3 ± 0.6	15 ± 2	37.1 ± 2.1	59 ± 3
(*R*)-1	H	CO	S	BOC	1.6 ± 0.2	108 ± 10	8.4 ± 0.2	17 ± 2	28.0 ± 1.0	35 ± 3
(*S*)-1	H	CO	S	BOC	i.a.	i.a.	i.a.	i.a.	i.a.	i.a.
2	Cl	CO	S	BOC	0.37 ± 0.06	95 ± 13	3.2 ± 1	10 ± 3	i.a.	i.a.
3	CH_3O	CO	S	BOC	0.38 ± 0.06	99 ± 6	7.5 ± 3.5	12 ± 2	i.a.	i.a.
4	CH_3	CO	S	BOC	0.94 ± 0.24	89 ± 12	4.6 ± 2.4	17 ± 4	i.a.	i.a.
5	NO_2	CO	S	BOC	4.8 ± 2.1	103 ± 30	12.8 ± 3.5	14 ± 2	i.a.	i.a.
6	CF_3	CO	S	BOC	0.25 ± 0.04	77 ± 19	2.2 ± 0.9	17 ± 4	i.a.	i.a.
7	H	CH_2	S	BOC	0.58 ± 0.17	64 ± 1	3.4 ± 0.5	14 ± 11	i.a.	i.a.
8	H	bond	S	BOC	0.71 ± 0.27	108 ± 2	3.9 ± 1.2	21 ± 11	i.a.	i.a.
9	H	CO−CH=CH	S	BOC	0.8 ± 0.5	94 ± 15	10.2 ± 2.5	30 ± 2	i.a.	i.a.
10	H	CO	O	BOC	12.1 ± 1.6	49 ± 4	20 ± 2	15 ± 2	i.a.	i.a.
11	H	CH_2	O	BOC	10 ± 4	52 ± 7	i.a.	i.a.	i.a.	i.a.
12	H	bond	O	BOC	7.2 ± 0.1	100 ± 18	13.0 ± 2.8	20 ± 6	i.a.	i.a.
13	H	CO	S	H	i.a.	i.a.	i.a.	i.a.	i.a.	i.a.
14	H	CO	S	Acetyl	i.a.	i.a.	i.a.	i.a.	i.a.	i.a.
15	H	CO	S	Benzoyl	i.a.	i.a.	25 ± 16	21 ± 13	i.a.	i.a.
16	H	CO	S	CBz	1.9 ± 0.8	90 ± 3	7.9 ± 1.2	22 ± 12	i.a.	i.a.
17	Cl	CH_2	S	CBz	0.016 ± 0.002	165 ± 11	i.a.	i.a.	i.a.	i.a.
18	Cl	bond	S	CBz	0.135 ± 0.015	138 ± 4	i.a.	i.a.	i.a.	i.a.
Wy-14,643					1.56 ± 0.3	100 ± 10	i.a.	i.a.	i.a.	i.a.
Rosiglitazone					i.a.	i.a.	0.04 ± 0.02	100 ± 9	i.a.	i.a.
L-165,045					i.a.	i.a.	i.a.	i.a.	0.021 ± 0.04	100 ± 4

i.a.: inactive at tested concentrations.

suggesting that this compound might activate a specific transcriptional program in steatotic HepaRG cells that results in an efficient reduction of lipid accumulation. To further characterize the pharmacological profile of (*R*)-**1**, we finally assessed its activity on glucose uptake from C2C12 muscle cells showing its ability to improve insulin sensitivity. Therefore, these results demonstrate that (*R*)-**1** may represent the potential lead of a new class of drugs for treatment of dyslipidemic type 2 diabetes.

1.1. Chemoinformatics search for PPAR ligands

To find structurally similar compounds to AL26, a previously reported PPARα/γ dual agonist [20], we built a SMARTS based query to screen the NCI Open Database (see Experimental Section and Fig. S2 for details) by means of RDKit nodes implemented in KNIME. Before screening, the database was extensively filtered to remove compounds with undesirable functionalities and retain those with drug-like properties. The substructure search identified 72 compounds that were clustered on the basis of the Morgan circular fingerprints (radius 2) similarity. This procedure allowed to easily select and acquire, taking into account compounds' availability, 16 compounds for biological testing (Table S1, Supporting Information). The 16 selected compounds were further checked for known classes of pan-assay interference compounds (PAINS) by using FafDrugs4 [21]. None of the compounds was found as potential PAINS and none of them exhibited violations of the "rule of 5" [22].

1.2. Biological testing of the selected compounds

AL26 analogues were evaluated in vitro for their agonist activity towards the human PPARα (hPPARα), PPARγ (hPPARγ), and PPARδ (hPPARδ) subtypes by employing GAL4-PPAR transactivation assay. For this purpose, GAL4-PPAR chimeric receptors were expressed in transiently transfected HepG2 cells according to a previously reported procedure [23]. In particular, the results obtained were compared with corresponding data for Wy-14,643, rosiglitazone, and L-165,041 used as reference compounds in the PPARα, PPARγ, and PPARδ transactivation assays, respectively. Maximum obtained fold induction with the reference agonist was defined as 100%.

Only three analogues showed activity toward PPARs and their potency and efficacy are reported in Table 1 in comparison with AL26. The first two of them, AL26-7 and AL26-11, were PPARα/γ dual agonists very similar to AL26 even though AL26-7 exhibited partial instead of full agonism toward PPARα. By contrast, the presence of a benzoyl group in the para-position of the S-benzyl moiety of AL26 as well as the introduction of a *t*-butyloxy group as a replacement for the benzyl bound to the amidic function led to the PPARα/γ/δ pan-agonist AL26-18 with a moderate and balanced activation profile.

Given that the activation of all three PPAR subtypes is currently considered a very attractive option for the development of antidiabetic drugs [13–16], we decided to design and synthesize a novel series of AL26-18 derivatives (Table 2) in which we studied the structure-activity relationship correlated to modifications introduced in different parts of the scaffold.

1.3. Chemistry

The synthesis of compounds **1**–**12** is depicted in Scheme 1 and was carried out starting from the appropriate 4-substituted benzyl bromides **19**–**27**. For the target acids **1**–**3**, **7**, **8**, and **10**–**12**, the corresponding benzyl bromides **19**–**21** or **25**, **26** were reacted with N-Boc-D,L-cysteine or serine in the presence of NaH in dry DMF. In the same way, the two enantiomers **(*R*)-1** and **(*S*)-1** were obtained starting from N-Boc-L-cysteine or N-Boc-D-cysteine, respectively. This procedure failed for the preparation of **4**–**6** and **9** which were alternatively synthesized by condensation of benzyl bromides **22**–**24** or **27** with D,L-cysteine and subsequent treatment of the intermediates **28**–**31** with di-tert-butyl dicarbonate in the presence of triethylamine.

Benzyl bromides were prepared as reported in Scheme 2 (only **19** and **26** were commercially available). Bromides **20**–**24** were obtained starting from the corresponding 4-substituted acyl chlorides which were condensed with toluene in the presence of $AlCl_3$; the intermediates **32**–**36** were then treated with N-bromosuccinimide in the presence of catalytic amounts of benzoyl peroxide to give the desired compounds. This last step was carried out, also, to prepare **27** by bromination of the chalcone intermediate **37** which, in turn, was obtained by condensation of acetophenone with 4-tolualdehyde. Finally, bromide **25** was synthesized by reduction of benzophenone **19** with triethylsilane and trifluoroacetic acid.

The synthesis of compounds **13**–**16** is reported in Scheme 3. The target acid **13** was obtained by condensation of **20** with D,L-cysteine and was also an intermediate for the preparation of **14**–**16** by reaction with acetyl chloride, benzoyl chloride or benzyl chloroformate, respectively.

Finally, in Scheme 4 the synthesis of compounds **17**–**18** is displayed. The procedure involved the two key intermediates **38** and **39** which were prepared in different ways. The former was obtained by reduction under mild conditions of benzophenone **19** as reported above for **25**; instead, the latter was prepared by condensation of 4-chloro-benzeneboronic acid with 4-bromotoluene under Suzuki cross-coupling conditions to give **40** whose bromination with N-bromosuccinimide in the presence of catalytic amounts of benzoyl peroxide allowed to obtain **39**. Benzyl bromides **38** and **39** were then reacted with N-Cbz-D,L-cysteine, obtained from D,L-cystine according to a procedure reported in the literature [24], to give the target acids **17** and **18**, respectively.

1.4. Biological activity of AL26-18 derivatives

Compounds **2**–**18** were evaluated in vitro for their agonist activity toward the human PPARs using the same procedure reported above.

1.4.1. Introduction of substituents on the distal ring of benzophenone

The PPAR activity of racemates **2**–**6** was examined first. The introduction of substituents with different stereo-electronic properties in the para position of the distal benzene ring of benzophenone moiety basically gave potent PPARα full agonists. With the exception of the nitro-substituted derivative **5**, all compounds displayed 4- to 7-fold higher potencies compared to **1** with the trifluoro-derivative **6** being the most potent (EC_{50} = 0.25 μM). Interestingly, the derivatives endowed with the highest potency (**2**, **3**, **4**, and **6**) were also potent PPARγ partial agonists indicating that the introduction of an appropriate substituent in the distal benzene ring of the benzophenone moiety provided the suitable structural requirements for the activation of both PPARα and PPARγ. The trifluoro-derivative **6** was still the most potent (EC_{50} = 2.2 μM) suggesting that both electron-withdrawing and lipophilic properties could be favorable for the interaction with this part of the receptor pocket. Surprisingly, none of these derivatives showed activity on PPARδ allowing to hypothesize the accommodation of the benzophenone moiety in a cleft of this receptor subtype which is too small to host any kind of substituent on the distal benzene ring.

1.4.2. Modification of the linker between the phenyl rings

As regards PPARα activity, the reduction of the carbonyl group of **1** to methylene gave the partial agonist **7** with 3-fold higher potency compared to **1**, whereas the removal of the carbonyl afforded the potent full agonist **8**. The insertion of a double bond in the benzophenone nucleus gave the vinylogous calchone derivative **9** with full agonist activity and potency 2-fold higher than **1**. All these compounds acted as partial agonists of PPARγ with **7** and **8** showing 3-fold higher potency than **1**. As regards PPARδ activity, no effects were observed on this receptor subtype.

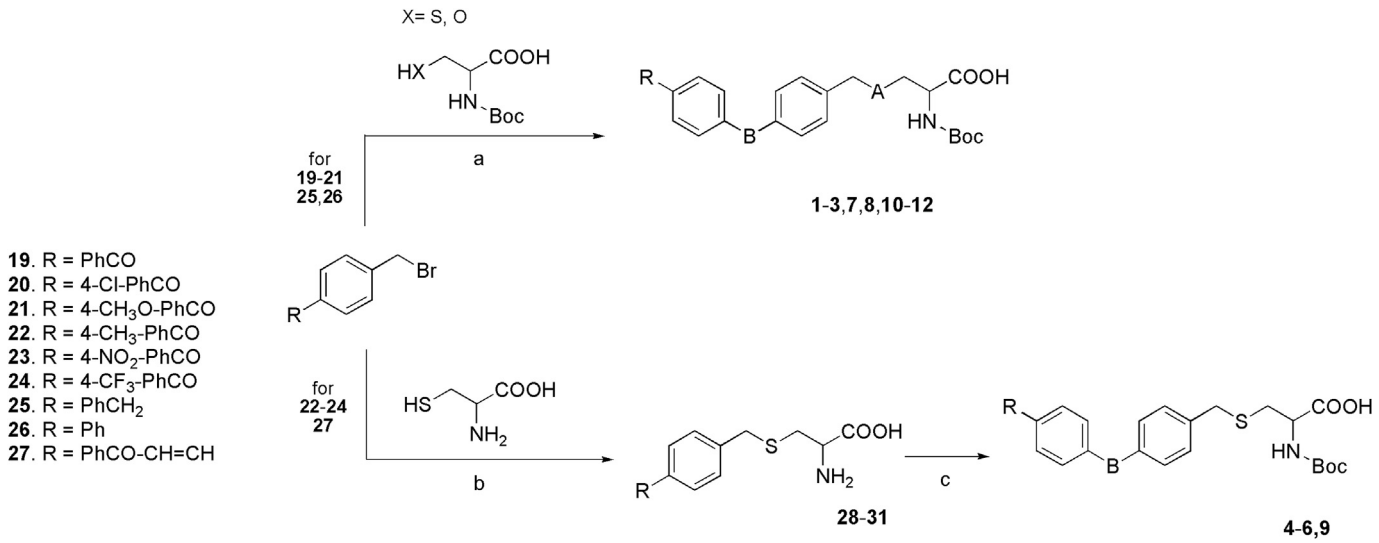

Scheme 1. a) NaH, dry DMF, N_2, 0 °C → rt, 24 h; b) 2 N NaOH/EtOH, rt, 30 min; c) H_2O/dioxane, TEA, Boc_2O, rt, 4 h.

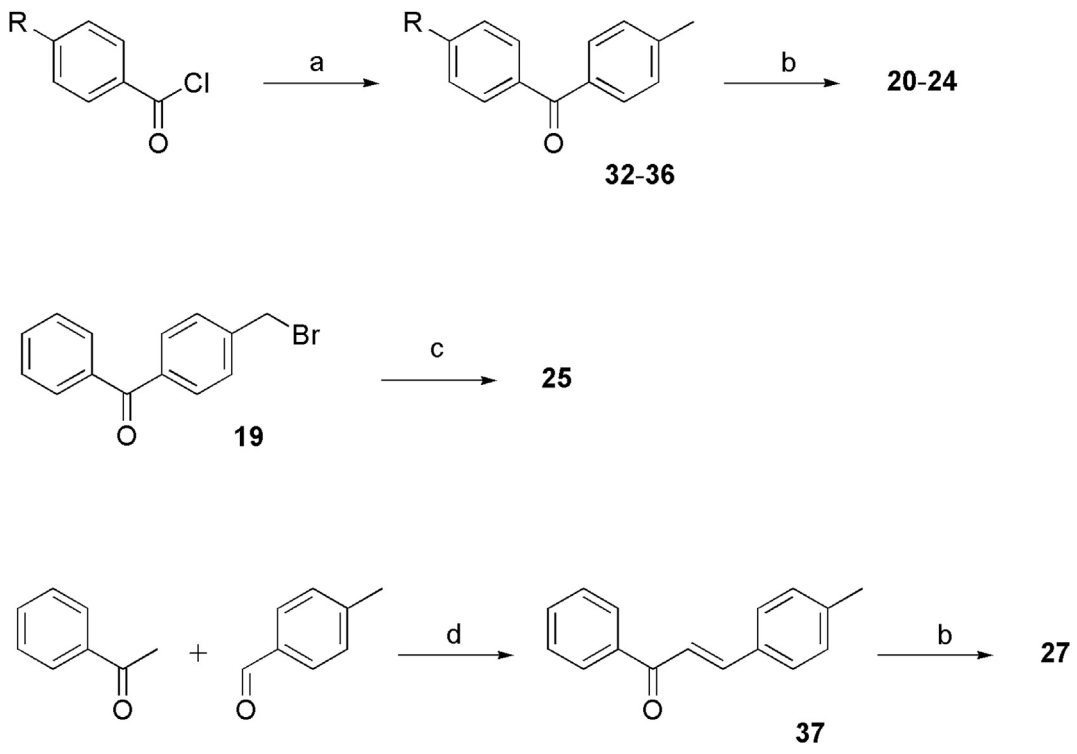

Scheme 2. a) Toluene, $AlCl_3$, rt, 1–2 h; b) N-bromosuccinimide, benzoyl peroxide, CCl_4, reflux, 5–7 h; c) Et_3SiH, CF_3COOH, N_2, 60 °C, overnight; d) 3 N NaOH/EtOH, rt, 2 h.

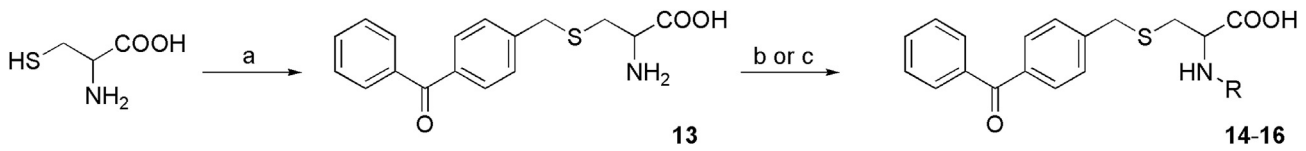

Scheme 3. a) **19**, 2 N NaOH/EtOH, rt, 30 min; b) H_2O/dioxane, 2 N NaOH, acetyl chloride, 0 °C → rt, 30min; c) 2 N NaOH, benzoyl chloride or benzyl chloroformate, 0 °C, 5 h.

1.4.3. Isosteric substitution of sulfur

Unexpectedly, this substitution resulted detrimental for activity. As regards PPARα, in fact, the replacement of sulfur with oxygen in compounds **1**, **7** and **8** resulted in isosteric derivatives endowed with significantly lower potency (7-fold for **10** vs **1**, 20-fold for **11** vs **7**, 10-fold for **12** vs **8**) but similar efficacy, except for compound **10** behaving as a partial agonist compared to the full agonist **1**. PPARγ activity, also, resulted lower than the corresponding sulfur isosteres

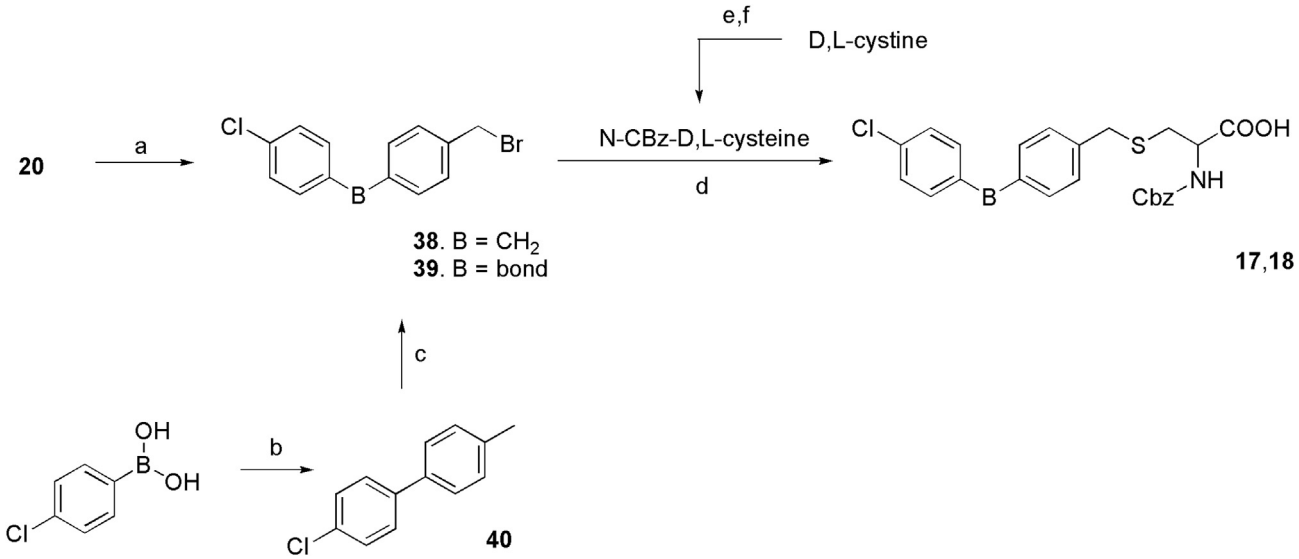

Scheme 4. a) Et_3SiH, CF_3COOH, N_2, 60 °C, overnight; b) 4-bromo-toluene, $Pd(AcO)_2$, TBAB, K_2CO_3, PEG400, 100 °C, overnight; c) N-bromosuccinimide, benzoyl peroxide, CCl_4, reflux, overnight; d) NaH, dry DMF, N_2, 0 °C → rt, 24 h; e) benzyl chloroformate, NaOH, H_2O/THF, 0 °C, 3 h; f) PPh_3, H_2O/THF, rt, overnight.

with compound **11** completely inactive. On the whole, it seems reasonable to assert that the presence of an oxygen atom in this part of the molecule reduces the activity probably due to unfavorable electrostatic interactions. Still, these compounds did not show any PPARδ activity either.

1.4.4. Different substitution of nitrogen

Compounds **13**–**16** were obtained by removing the Boc group of **1** to give the corresponding amino analog (**13**) or by replacement of t-butoxy with methyl (**14**), phenyl (**15**) or benzyloxy group (**16**). The first two compounds resulted completely inactive towards all of three receptor subtypes, whereas the benzoyl derivative **15** showed a moderate activity on PPARγ. Only the introduction of the benzyloxycarbonyl group (**16**) restored the same activity of reference compound **1** on PPARα and PPARγ. In this case, also, as for all the other modifications of compound **1**, PPARδ activity was still lacking.

Finally, we tested compounds **17** and **18** in which we introduced all the structural modifications that seemed to confer the best pharmacological requirements to this series of analogues. Indeed, these two compounds turned out to be highly selective and very potent full PPARα agonists with EC_{50} 16 nM and 135 nM, respectively (seeTable 2).

1.4.5. Absolute configuration of stereogenic center

PPARs show a high degree of stereoselectivity towards several classes of drugs. In particular, PPAR activity is strongly affected by the presence of a stereogenic center close to a carboxylic function which, therefore, plays a crucial role in determining the PPAR binding mode. For this reason, we prepared the two enantiomers of compound **1** and tested them in transactivation assay. As expected, a very high eudismic ratio was observed; infact, the activity resided only in the R stereoisomer, whereas (*S*)-**1** resulted completely inactive towards all of three subtypes (Fig. 2).

1.5. Effects of (R)-1 on steatosis and gene expression

To further characterize the pharmacological profile of (*R*)-**1**, we decided to evaluate its activity on steatosis induced by oleic acid overload in differentiated human HepaRG cell line that is considered one of the best models for pharmacological and toxicological tests on human hepatic cells in vitro. These cells have been extensively characterized for their ability to differentiate into both biliary and hepatocyte lineages in the presence of DMSO [25]. In addition, they retain the major functional activities of human primary cells, including the expression of key hepatic transcription factors such as PXR, CAR and also PPARs [26,27]. The results were compared with those obtained from fenofibrate and rosiglitazone which were used as reference ligands. To assess their maximal effect, all compounds were used at high, but not toxic (data not shown) concentrations, corresponding to at least 10 times the EC_{50}. Steatosis was induced in differentiated HepaRG cells by oleic acid overload for 24 h, as previously described [28]. The effects of (*R*)-**1** were evaluated after acute (24 h) and repeated treatments (15 days), always in presence of oleic acid (Fig. 3A and E). As depicted in Fig. 3B and C, the treatment with (*R*)-**1** for 24 h significantly reduced lipid accumulation in HepaRG cells, while with fenofibrate and rosiglitazone the slight reduction did not reach statistical significance. When HepaRG cells were chronically treated with PPAR ligands, in presence of oleic acid (Fig. 3E), the effects of the different compounds were more pronounced. Indeed, all tested ligands significantly counteracted lipid accumulation induced by oleic acid, as shown in Fig. 3F and G. To investigate the mechanisms underlying such improvement of hepatosteatosis, we selected a panel of PPAR target genes with key roles in the regulation of lipid metabolism in hepatic cells. Gene expression analysis revealed a strong induction of the mRNA levels of hydroxymethylglutaryl-CoA synthase 2 (HMGCS2), fibroblast growth factor 21 (FGF21), pyruvate dehydrogenase kinase 4 (PDK4) and fatty acid binding protein 1 (FABP1) by acute (*R*)-**1** treatment, in agreement with its activity on both PPARα and PPARγ receptors (Fig. 3D). In contrast, no effect was detected on the expression of liver carnitine palmitoyl-transferase (CPT1a) and the ATP-binding cassette transporter A1 (ABCA1). Of note, (*R*)-**1** was the only ligand able to induce both FGF21 and FABP1 in these experimental conditions. Interestingly, the gene expression profile in response to chronic treatment with fenofibrate, rosiglitazone and (*R*)-**1** showed a differential activation of the selected target genes, with (*R*)-**1** inducing CPT1a, HMGCS2, FGF21 and FABP1, while fenofibrate was particularly active on PDK4 and rosiglitazone only on FABP1 (Fig. 3H).

These results suggest that these compounds might activate a specific transcriptional program in steatotic HepaRG cells that results in an efficient reduction of lipid accumulation. With regards to

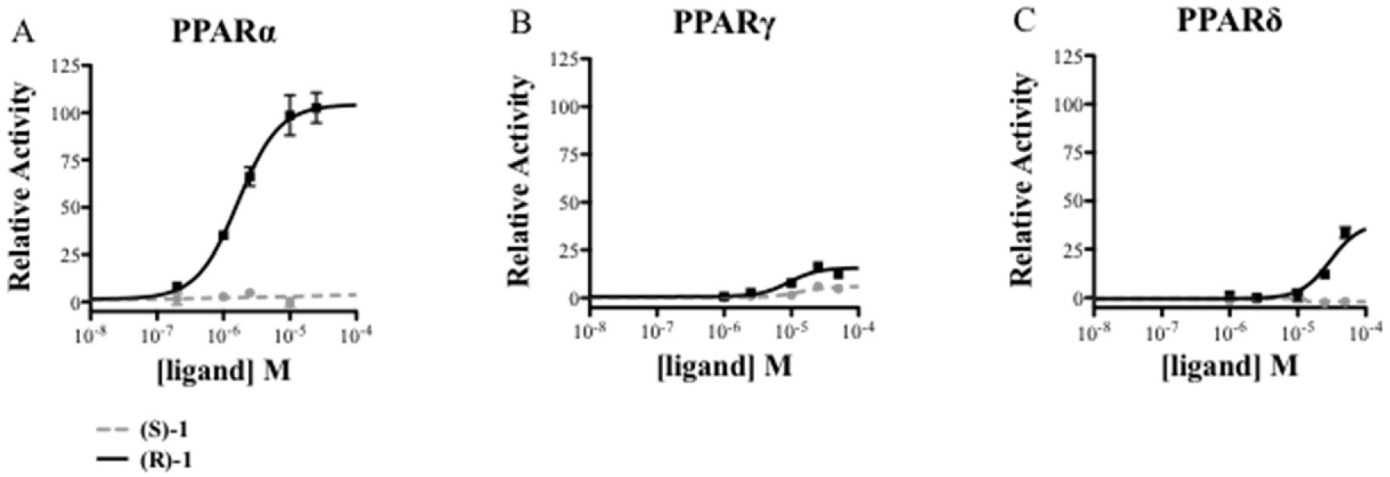

Fig. 2. Luciferase reporter assay showing the concentration-dependent effects of (*R*)-**1** and (*S*)-**1** on PPARα (A), PPARγ (B), and PPARδ (C) transactivation.

(*R*)-**1** activity, this ligand is particularly active on genes involved in fatty acid oxidation and ketogenesis (CPT1a and HMGS2, respectively), whose activation suggests an increased capacity of cells to metabolize fatty acids. Further supporting this effect, (*R*)-**1** strongly induces the expression of FABP1, which facilitates the uptake of long chain fatty acids from membranes and binds them, thus minimizing their cytotoxic detergent effects and functioning as a donor for both peroxisomal and mitochondrial β-oxidation [29]. Acute, but not chronic treatment with (*R*)-**1** also induces the mRNA levels of PDK4, a controller of the fuel switching between glucose and free fatty acids [30], whose upregulation is, however, associated to obesity, diabetes and NAFLD [31]. In this sense, the lack of induction of PDK4 following chronic treatment with (*R*)-**1** might have beneficial pharmacological implications. Finally, (*R*)-**1** strongly increases the expression of FGF21, which might be associated to favorable metabolic outcomes. Indeed, FGF21, whose production is mainly hepatic, has a plethora of metabolic effects, including suppression of lipogenesis which redirects fatty acids to β-oxidation [32], activation of PPARγ coactivator 1α, which regulates hepatic glucose and lipid metabolism [33], and improvement of insulin sensitivity [34].

Compared to fenofibrate and rosiglitazone, used as reference PPARα and PPARγ activators, (*R*)-**1** shows an enhanced ability to induce the expression of several target genes. This is due, at least in part, to its concomitant effect on all PPAR isoforms at the tested concentrations. However, in some case, a gene-specific effect seems to be present, which reinforces the notion that the activation of the same PPAR subtype by different agonists does not necessarily lead to similar outcomes. Further studies will be necessary to investigate the molecular basis of such differences and their possible consequences at pharmacological level.

1.6. Effects of (R)-1 on glucose uptake

The strong increase of the expression of FGF21 with its known metabolic effect of improving insulin resistance prompted us to test the insulin-sensitizing effect of (*R*)-**1** by investigating its ability to increase glucose uptake in C2C12 muscle cells. Skeletal muscle is a primary site of glucose uptake and disposal after meal and, therefore, plays a crucial role in the maintenance of glucose homeostasis. As shown in Fig. 4, compared to rosiglitazone, (*R*)-**1** treatment improved glucose uptake, suggesting that, after chronic stimulation, muscle cells were capable to acquire glucose more efficiently. Interestingly, combination of (*R*)-**1** with insulin enhanced this uptake further, allowing the stimulation by insulin to be more effective in terms of glucose absorption. These results allow to hypothesize that the strong increase of the expression of FGF21 is probably responsible of the improved insulin resistance even though we cannot rule out the possible involvement of other specific factors. At this point, in an attempt to explain the mechanism responsible of the increased glucose uptake in muscle cells, we decided to verify if the expression of GLUT4, the main glucose transporter through cell membrane, was affected from our compound (*R*)-**1**. To this end, murine myoblasts were treated with rosiglitazone (10 μM) and (*R*)-**1** (25 μM) for 96 h after which the cells were lysed and the expression level of GLUT4 was evaluated by Western blot analysis. Surprisingly, we observed that treatment with either drug did not cause a significant increase in GLUT4 expression (Fig. 5). This finding suggests that the increased glucose uptake is mainly due to stimulation of GLUT4 translocation from the intracellular compartment to the plasma membrane rather than to upregulation of protein expression. Similar results have been previously described for brown adipocytes treated with rosiglitazone [35].

1.7. Docking studies

In order to clarify the possible binding mode of this series of compounds and to help interpretation of SAR data, we undertook docking studies using the Glide module [36,37], which is part of the Maestro software suite (Maestro, Schrödinger, LLC, New York, NY, 2020), with the X-ray structures of PPARα in complex with fenofibric acid (PDB 7BQ0) [38], PPARγ in complex with the partial agonist GL479 (PDB 4CI5) [39], and PPARδ in complex with the ligand 6-(2-((N-cyclopropyl-4-(furan-2-yl)benzamido)methyl) phenoxy)hexanoic acid (PDB 5U3Q) [40].

PPARα, -γ, and -δ share a "Y shaped" ligand binding domain (LBD), which is composed of a polar arm I extending toward H12, a hydrophobic arm II, which is located between H3 and the β-sheet, and a hydrophobic entrance (arm III).

Compound (*R*)-**1**, which turned out to be the active enantiomer in transactivation assays, occupies mostly arm I in PPARα, making conventional interactions with the polar side chains of S280, Y314, H440, and Y464 (Fig. 6A–C). Superposition of the docking pose of (*R*)-**1** over the co-crystallized fenofibric acid in Arm I showed a good overlap of both carboxylic groups and benzophenone moieties (Fig. S1, Supporting Information). In particular, the aromatic benzophenone moiety fills the hydrophobic region between H3,

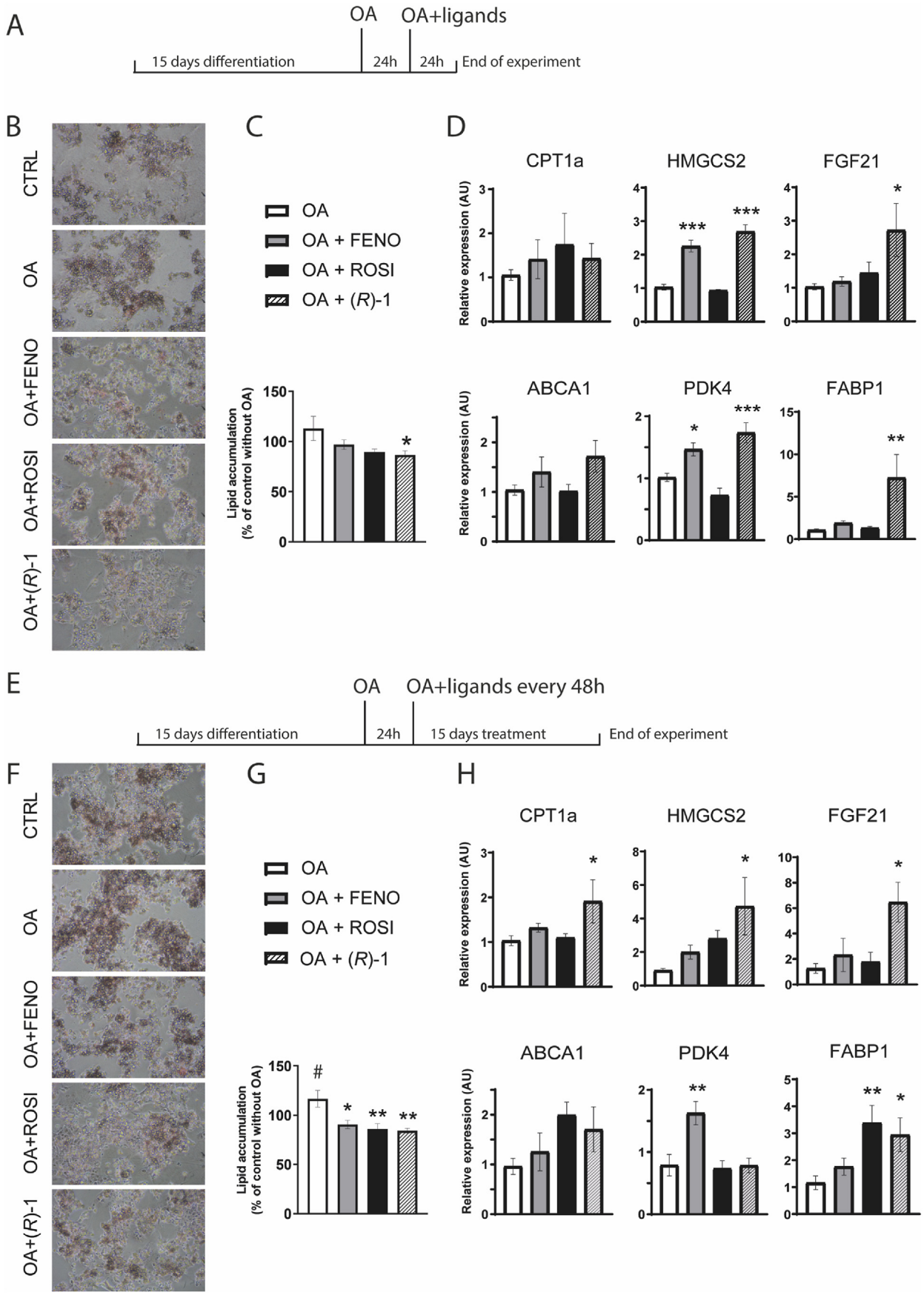
A
OA
OA+ligands
15 days differentiation
24h
24h
End of experiment
B
CTRL
OA
OA+FENO
OA+ROSI
OA+(R)-1
C
OA
OA + FENO
OA + ROSI
OA + (R)-1
Lipid accumulation (% of control without OA)
D
CPT1a
HMGCS2
FGF21
ABCA1
PDK4
FABP1
Relative expression (AU)
E
OA
OA+ligands every 48h
15 days differentiation
24h
15 days treatment
End of experiment
F
CTRL
OA
OA+FENO
OA+ROSI
OA+(R)-1
G
OA
OA + FENO
OA + ROSI
OA + (R)-1
Lipid accumulation (% of control without OA)
H
CPT1a
HMGCS2
FGF21
ABCA1
PDK4
FABP1
Relative expression (AU)

H11 and H12: a similar situation was also observed in the complex of PPARα with AL29-26 [20]. The ligand Boc group forms additional hydrophobic interactions with I317, F318, L321 on H5.

Compound (*R*)-**1** showed a different binding mode into PPARγ LBD as compared to that of PPARα, lacking a direct interaction with H12. This binding mode would be in line with many reported partial agonists, which are mainly positioned within arm III and tend rather to stabilize the β-sheet [12,41]. In fact, the carboxylate group of (*R*)-**1** accepted an H-bond from the backbone NH of S342 side chain located on the β-sheet and also formed a salt bridge with the Nε of R288 side chain on H3 (Fig. 7A–C). The Boc group formed hydrophobic contacts with I326, M329, L330, on H5, L333 on the β-sheet. The benzophenone group stretched along H3, with the carbonyl forming a weak interaction with the side chain of Y327 (distance of 3.9 Å) and the distal aromatic ring forming an edge-to-face π-π stacking interaction with H449 side chain on H11.

As regards PPARδ, (*R*)-**1** docked pose was preferentially located between H3 and the β-sheet, lacking an interaction with Y437 on H12, an important residue for the potency of PPARδ agonists. Instead, the ligand carboxylate group formed a salt bridge with the side chain of K229 on H2′-H3 loop of PPARδ-LBD, as well as an H-bond with the backbone nitrogen atom of N307 on the β-sheet (Fig. 7B–D). The remainder of the ligand established mostly hydrophobic interactions: the Boc group with M293, whereas the benzophenone group with L294 on H5, I327, K331, F332 on H7, V305 on the β-sheet and C249 on H3, and possibly engaging a further interaction with the side chain of T253 by its carbonyl group (albeit with a longer distance of 3.5 Å). Therefore, the low affinity and the attenuated transcriptional response of (*R*)-**1** toward PPARδ might be ascribed to such peculiar binding mode.

On the contrary, the (*S*)-**1** enantiomer resulted inactive at the three PPAR subtypes; docking experiments revealed that the inversion of chirality dramatically changed the binding mode of this ligand. The overlay of (*R*)-**1** and (*S*)-**1** docked poses into PPARα (Fig. S1) showed that the (*S*)-**1** Boc group was placed within Arm I, whereas the benzophenone group was projected toward H3; taking into account the cocrystallized pose of fenofibric acid, in which the same moiety binds in the opposite direction, we might infer that this moiety would be less likely accommodated within the PPARα LBD in this orientation, likely affecting the ligand's binding affinity. The (*S*)-**1** enantiomer assumed a "flipped" orientation into PPARγ with respect to (*R*)-**1**, causing the carboxylate group to be shifted downwards, toward H7, and thus losing the important contacts with H3 and the β-sheet. A similar outcome was observed also in PPARδ: (*S*)-**1** wrapped around H3 but lacking significant interactions and thus causing a definitive drop in binding affinity.

The binding mode of (*R*)-**1** suggested that both PPARα and PPARγ can easily accommodate small and lipophilic substituents at the para position of the distal benzene ring of benzophenone.

PPARα in particular favored derivatives bearing the trifluoromethyl (**6**) and chlorine (**2**), in line with the presence of a chlorine atom in the same position of the fenofibric acid (Fig. S1). These groups are tightly enclosed in a hydrophobic pocket. Thereby, the nitro-substituted derivative **5** would not be able to fit the hydrophobic pocket in a similar fashion, which explains its weaker activity and efficacy. A similar reasoning can be derived for PPARγ as well, since the substituents in para would be surrounded by hydrophobic residues such as L469, L453 and F282.

Instead, the para-substituted derivatives **2** and **3**–**6** could not be hosted in PPARδ because the hydrophobic cleft in which the benzophenone projects is rather smaller and steric clashes likely occur with residues of H7, in particular I328, K331 and F332.

Modifications on the carbonyl group of the benzophenone moiety improved the activity on PPARα, and to a similar extent also on PPARγ (derivatives **7**–**9**), consistent with the fact that there is room in their LBDs for bulkier terminal groups, either in a bent or straight conformation.

The isosteric replacement of the sulfur atom with oxygen (compounds **10**–**12**) provoked a drop in potency toward PPARα and PPARγ, whereas the activity was completely lost in PPARδ. The sulfur to oxygen switch leads to an inversion of the chirality on the stereogenic center close to the carboxylic group, which likely has a negative impact on the binding mode of these compounds. Indeed, the activity is highly dependent on enantiomeric preference, as observed with (*R*)-**1** and (*S*)-**1**. Moreover, the presence of the oxygen could induce the carboxylic group to assume a less favorable conformation for H-bonds formation.

The effect of protective groups different than Boc on the nitrogen atom yielded interesting outcomes: the amino and acetylated derivatives **13**–**14** resulted completely inactive toward the three receptor subtypes, because they lacked the hydrophobic interactions formed by Boc, which contributed proficiently to anchor the ligand in the appropriate conformation to activate the receptor. However, the optimal protective group would require, besides bulkiness and hydrophobicity, a certain degree of flexibility, as the benzoyl derivative **15** resulted completely inactive on PPARα and -δ, and much less active than (*R*)-**1** on PPARγ.

Compound **16**, bearing the more flexible benzyloxycarbonyl protective group, showed similar activity to (*R*)-**1** on PPARα and -γ but turned out to be inactive on -δ, due to the excessive bulkiness of this group which could not fit properly within the receptor.

The 4-Cl-substituted diphenylmethane and biphenyl derivatives **17** and **18** showed exquisite potency and selectivity toward PPARα. Hence, we undertook docking simulations for the most potent compound of the series, **17**. Since in vitro studies indicated that (*R*)-**1** is the eutomer for racemate **1**, docking of compound **17** was performed using the (*R*)-**17** enantiomer.

(*R*)-**17** formed tight interactions with the polar side chains of S280, Y314, H440, and Y464, as observed for (*R*)-**1** (Fig. 6B–D). Moreover, the 4-Cl atom was optimally oriented to form a halogen bond with the side chain of K448. The benzyloxycarbonyl moiety plunged into a hydrophobic area where it could engage sulfur-aromatic interactions with C276, M355, and M330, as also observed for previously reported PPARα ligands with high affinity [16]. This remarkable environment might justify the augmented potency of (*R*)-**17** toward PPARα with respect to -γ and -δ.

We also performed the *in silico* absorption, distribution, metabolism, and excretion-toxicity (ADMET) pharmacokinetics evaluation for the most promising compound (*R*)-**1** by means of the QikProp software (Schrodinger, LLC, New York, NY, 2020). The results of these calculations are reported in Table S2. The molecular properties of compound (*R*)-**1** showed satisfactory results, as the

Fig. 3. Biological activity of (*R*)-**1** in hepatic cells.
Experimental design. After two weeks of differentiation in medium supplemented with 2% DMSO, cells were treated with oleic acid (OA) 500 μM for 24 h to induce steatosis and then treated with the indicated ligand or vehicle, in presence of oleic acid, for additional 24 h (A) or 2 weeks (E). For chronic treatments the medium was replenished every two days. For HepaRG cells treated 24 h with the indicated ligands or vehicle, representative pictures of OilRedO staining are shown in (B), lipid quantification in (C) and gene expression of the indicated genes in (D). For HepaRG cells treated two weeks with the indicated ligands or vehicle, representative pictures of OilRedO staining are shown in (F), lipid quantification in (G) and gene expression of the indicated genes in (H). In panels (C) and (G) values are expressed as the percentage of lipid accumulation observed in control cells, not exposed to OA. OA bars are set to 1 in (D) and (H). FENO = fenofibrate 250 μM; ROSI = rosiglitazone 10 μM; (*R*)-**1** was used at 100 μM. Bars represent the mean ± SE of two independent experiments. #P < 0.05 versus control cells, not exposed to OA; *P < 0.05, **P < 0.01, ***P < 0.001 versus OA alone.

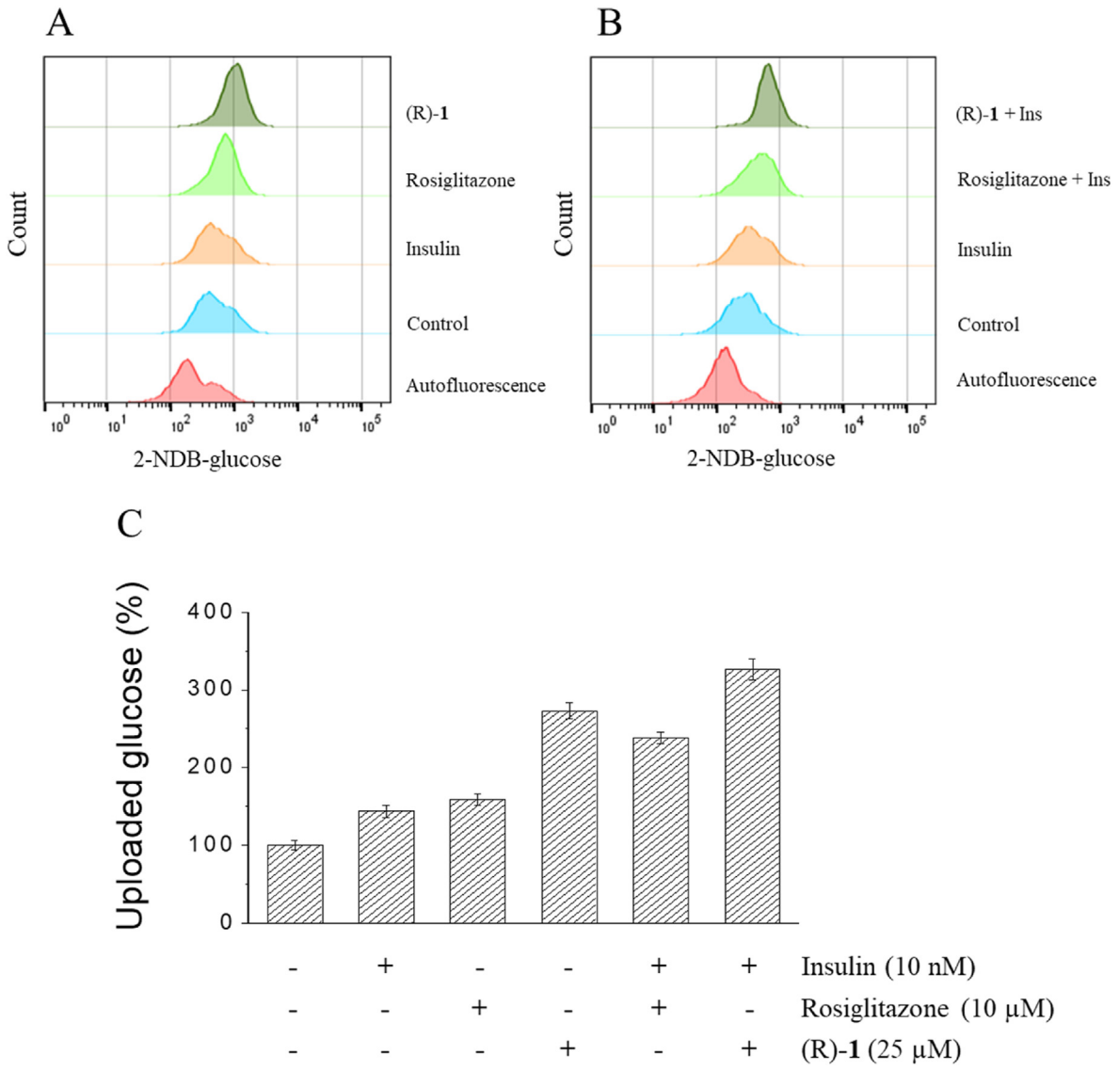

Fig. 4. Flow cytometry analysis of 2-NBDG uptake in C2C12 cells. Murine myoblasts were treated with rosiglitazone (10 μM) and (*R*)-**1** (25 μM) for 96 h in starvation medium. Each 24 h, treatment medium was renewed. After 96 h, cells were stimulated with insulin (10 nM) for 30 min before the analysis. Glucose uploaded was evaluated by using a flow cytometer apparatus (FACSCanto II, BD Biosciences, San Jose, CA, USA). Each test was carried out in triplicate. (A), C2C12 cells treated with rosiglitazone and (*R*)-**1** alone; (B) C2C12 cells pre-treated with rosiglitazone and (*R*)-**1** and then stimulated with insulin. (C), quantification of glucose uploaded. Data obtained were normalized respect to control test. Data showed represent the mean value ± S.E.M.

calculated properties fell within the ranges predicted by QikProp for 95% of known oral drugs, indicating the potential for further optimization as drug lead. Compound (*R*)-**1** displayed acceptable intestinal absorption, as predicted by the estimated Caco-2 cell permeability, as well as good predicted human oral absorption. (*R*)-**1** did not show potential hERG K^+ channel inhibition. No violation of Lipinski's rule of five was found.

2. Conclusion

In the present study, we performed a chemoinformatics search for PPAR ligands resulting in the selection of 16 compounds. Among them, we identified a novel PPARα/γ/δ pan-agonist with a moderate and balanced activation profile (AL26-18). The activity of AL26-18 prompted us to design and synthesize a novel series of derivatives in an attempt to investigate the effects resulting from its chemical modification and optimize the structure-activity relationships. Notably, two specific PPARα agonists with submicromolar potency, compounds **17** and **18**, emerged from this series. In addition, we prepared the two enantiomers of AL26-18 ((*R*)-**1** and (*S*)-**1**) and highlighted the strong influence of stereochemistry given that only the *R* enantiomer turned out to be active. Indeed, AL26-18 and (*R*)-**1** showed the same potency, but this could be due to the variability often displayed from biological assays carried out on cell lines. However, beyond the potency, many other advantages suggest to prefer a eutomer in place of racemic mixture. In fact, the eutomer of a drug is a single agent instead of a mixture of two distinct drugs, which simplifies the interpretation of the basic pharmacology, therapeutic and toxic effects, pharmacokinetic properties, and the relationship of plasma concentrations to effects. Docking studies were performed in order to clarify the possible binding mode of the whole series of compounds and to help

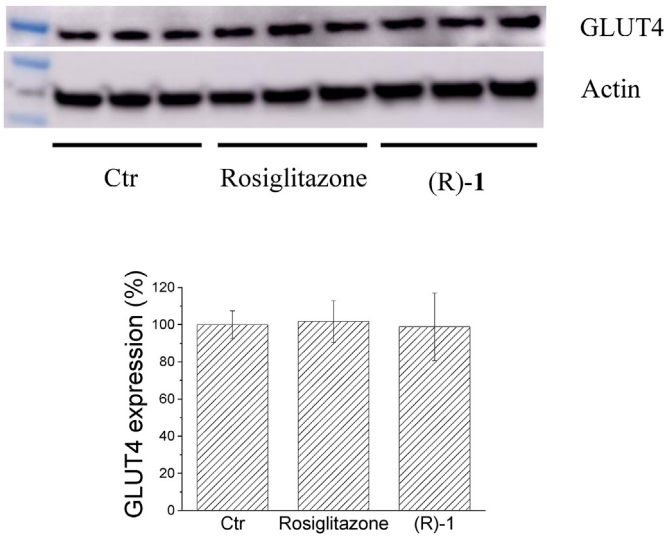

Fig. 5. GLUT4 expression level in muscle cells treated with rosiglitazone or (*R*)-1. Murine myoblasts were treated with rosiglitazone (10 μM) and (*R*)-1 (25 μM) for 96 h in starvation medium. Each test was performed in triplicate. Ctr: Control test. The data shown in the figure represent the mean value ± SD (n = 3).

interpretation of SAR data. To investigate further the biological properties of (*R*)-**1**, we next assessed its activity on steatotic HepaRG cells and demonstrated its ability to reduce lipid accumulation which is one of the major side effects of PPARγ full agonists like rosiglitazone. To explain the mechanisms underlying such improvement of hepatosteatosis, gene expression experiments on HepaRG cells were performed and the results showed an enhanced ability of (*R*)-**1** to induce the expression of several PPAR target genes suggesting that this compound might activate a specific transcriptional program in steatotic HepaRG cells that results in an efficient reduction of lipid accumulation. Our data show, indeed, that the effect on long term lipid accumulation of (*R*)-**1** is comparable to that of the positive control drugs. However, and importantly, the activation profile of the selected target genes is not the same and this might have important consequences in a therapeutic perspective. For instance, (*R*)-**1** does not induce PDK4, while it is the only ligand activating FGF21, likely due to its peculiar activity on PPAR subtypes. Such selective activation of FGF21 in hepatic cells could result systemically in increased circulating levels of this hormone, which has known insulin sensitizing effects in other tissues such as, for instance, muscle. For this reason, to further characterize the pharmacological profile of (*R*)-**1**, we finally assessed its activity on glucose uptake from C2C12 muscle cells. After chronic stimulation, muscle cells were capable to acquire glucose more efficiently. Interestingly, combination of (*R*)-**1** with insulin, enhanced this uptake further, allowing the stimulation by insulin to be more effective in terms of glucose absorption. Surprisingly, we observed that treatment with (*R*)-**1** did not cause a significant increase in GLUT4 expression suggesting that the increased glucose uptake is mainly due to stimulation of GLUT4 translocation from the intracellular compartment to the plasma membrane rather than to upregulation of protein expression. Further studies are needed to investigate the exact mechanism by which this ligand modulates the expression of the factors regulating lipid and carbohydrate metabolism. However, these results demonstrate the reliability of our chemoinformatics search approach for new PPAR ligands and allow to claim that (*R*)-**1** may represent a very promising candidate as the lead of a new class of drugs for treatment of dyslipidemic type 2 diabetes.

3. Experimental section

3.1. Computational chemistry

3.1.1. Chemoinformatics search

The NCI Open Database, containing ~260,000 compounds, was obtained from the website https://cactus.nci.nih.gov/download/nci/index.html#release-4.

The compound library was processed using the RDKit nodes implemented in KNIME (Konstanz Information Miner, version 3.3.2) [42]. Duplicates and compounds not able to be processed by the software were eliminated. To retain only druglike molecules, we applied a number of filters: first, we removed all molecules that contained an atom that was not in the set {H, C, N, O, F, P, S, Cl, Br, I}. Subsequently, we applied SMARTS based filtering patterns to remove compounds with undesirable properties [43,44], resulting in a new set of 195,241 compounds. This filtered database was exposed to a substructure search, using as query the following SMARTS notation: [#6](-[#6](-[#6](-[#8]-[#1]) = [#8])-[#7](-[#1])-[#6])-[#16]-[#6], corresponding to the core structure of compound AL26, which was previously reported to act as PPAR α/γ dual agonist in transactivation assays [20]. The substructure search yielded 72 compounds; to better analyze and organize this subset, we applied an agglomerative hierarchical clustering based on the Morgan circular fingerprints (radius 2), with a Tanimoto distance threshold of 0.5. Finally, 16 compounds were purchased or requested from the NCI Developmental Therapeutics Program (DTP) (Table S1) for biological evaluation. In addition to the above reported filtering procedure, the 16 selected compounds were further checked for known classes of pan-assay interference compounds (PAINS) by using Faf-Drugs4 [21]. None of the compounds was found as potential PAINS and none of them exhibited violations of the "rule of 5" [22].

The same procedure was employed to examine the synthesized compounds **1**–**18**; none of them was flagged as potential PAINS.

3.1.2. Protein and ligand preparation

The starting coordinates of PPARα in complex with fenofibric acid (PDB 7BQ0) [38], PPARγ in complex with the partial agonist GL479 (PDB 4CI5) [39], as well as PPARδ in complex with the ligand 6-(2-((N-cyclopropyl-4-(furan-2-yl)benzamido)methyl)phenoxy) hexanoic acid (PDB 5U3Q) [40], retrieved from Brookhaven Protein Database, were employed for the docking calculations.

The proteins were processed through the Protein Preparation Wizard in Maestro (Maestro, Schrödinger, LLC, New York, NY, 2020). X-ray water molecules were removed, the appropriate bond orders as well as charges and atom types were assigned, and the hydrogen atoms were added to the three protein structures. The H-bond network was optimized by exhaustive sampling of rotamers, tautomers and protonation states of titratable amino acids at neutral pH. Imidazole rings of H440 into PPARα, H449 and H323 into PPARγ, and H287 and H413 into PPARδ were set in their Nε 2-H (N tau-H) tautomeric state. Finally, the protein structures were relaxed by means of a restrained minimization using the Impref module with the OPLS3e force field, by imposing a 0.3 Å RMSD limit from the initial coordinates as constraint.

The chemical structures of the most relevant compounds, namely (*R*)-**1**, (*S*)-**1** and (*R*)-**17**, were manually built using the fragment dictionary of Maestro, before undergoing a ligand preparation workflow (LigPrep, Schrodinger, LLC, New York, NY, 2020). This involved ionization using Epik, in order to generate possible protonation states and tautomers at pH 7.0 ± 2.0. The compounds were then energetically minimized using the OPLS3e force field, and the resulting 3D structures used to specify chiral centers.

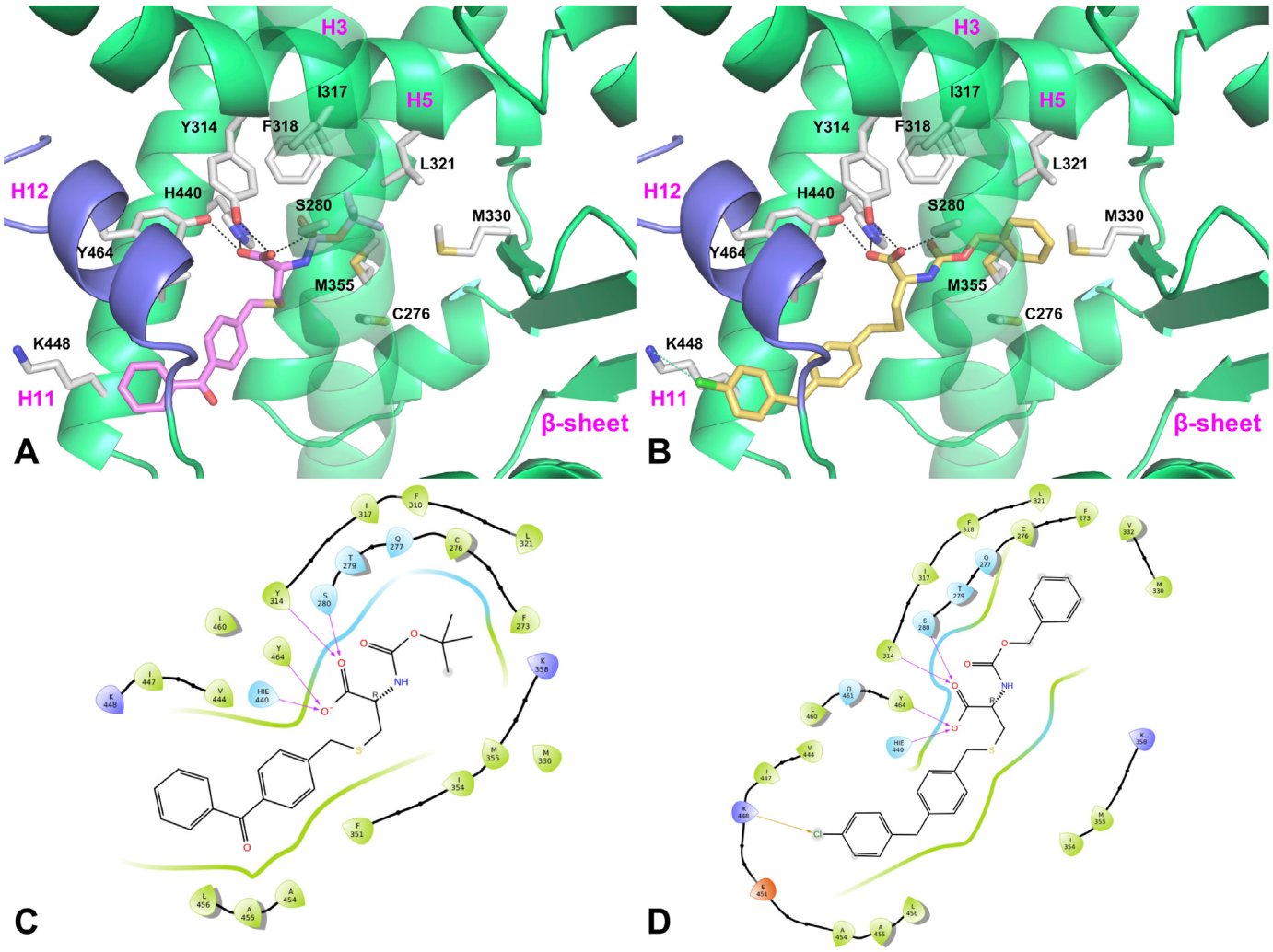

Fig. 6. Binding mode of compounds (*R*)-**1** (A, violet sticks) and (*R*)-**17** (B, yellow sticks) into PPARα (green ribbons, PDB 7BQ0) LBD. H12 is shown in slate. Only amino acids discussed in the main text are displayed (white sticks) and labeled. H-bonds discussed in the text are depicted as dashed black lines. The halogen bond of (*R*)-**17** in PPARα is highlighted as a green dashed line. 2D ligand interaction diagram of compounds (*R*)-**1** (C) and (*R*)-**17** (D) into PPARα LBD. Positively charged amino acids are represented with dark blue drops, negatively charged amino acids are represented with red drops, polar amino acids are represented with light blue drops and hydrophobic amino acids are represented with green drops. H-bonds are depicted with purple arrows. Straight green lines represent π-stacking interactions. Straight blue-red lines represent salt bridges. Straight light brown lines represent halogen bonds.

3.1.3. Docking simulations

Docking of (*R*)-**1**, (*S*)-**1** and (*R*)-**17** was performed with the Glide algorithm in Standard Precision (SP) mode [36,37]. A docking grid was generated, enclosing a box centered on the co-crystallized ligands, namely GL479 for PPARγ, 6-(2-((N-isopropyl-[1,1′-biphenyl]-4-carboxamido)methyl)phenoxy)hexanoic acid for PPARδ, with a dimension of 10 × 10 × 10 Å. For PPARα, since the fenofibric acid was found to have two binding sites in Arm I and Arm II, a larger docking grid was generated on the first molecule bound in Arm I, with dimension of 20 × 20 × 20 Å enclosing both sites. A scaling factor of 0.8 was set for van der Waals radii of receptor atoms. Ligand sampling was allowed to be flexible. Default docking parameters were used, and no constraints were included. At most ten docking ligand poses were retained per run and ranked using the GlideScore function [36,37]. After post-docking minimizations, the top binding pose for each ligand was inspected for key interactions using Maestro and ligand interaction diagrams. Binding poses were selected on the basis of the scoring, the similarity to the co-crystallized ligand binding mode and the consistency of protein-ligand interactions with the experimental data.

Before proceeding with the docking studies of the compounds under study, we investigated pose generation quality by re-docking the co-crystallized ligands back to their respective receptors. The software well reproduced the experimental geometries, with RMSD values of 0.37, 1.01, and 0.46 for PPARα, -γ, and -δ respectively.

3.2. Chemistry

3.2.1. General procedures

Commercially available chemicals were obtained from Sigma Aldrich Chemicals (Milan, Italy) and were used as purchased, without further purification. Reactions were monitored via Thin Layer Chromatography (silica gel, UV254) with UV light (short wave ultraviolet 254 nm and long wave ultraviolet 365 nm). Reactions carried out in anhydrous condition were performed under argon or nitrogen atmosphere. Column chromatography was performed using Fluka silica gel 60 Å (63–200 μM). Mass spectra were recorded on a HP MS6890-5973 MSD spectrometer, electron impact 70eV, equipped with a HP ChemStation, or on an Agilent LC-MS 1100 Series LC-MSD Trap System VL, spectrometer, electrospray

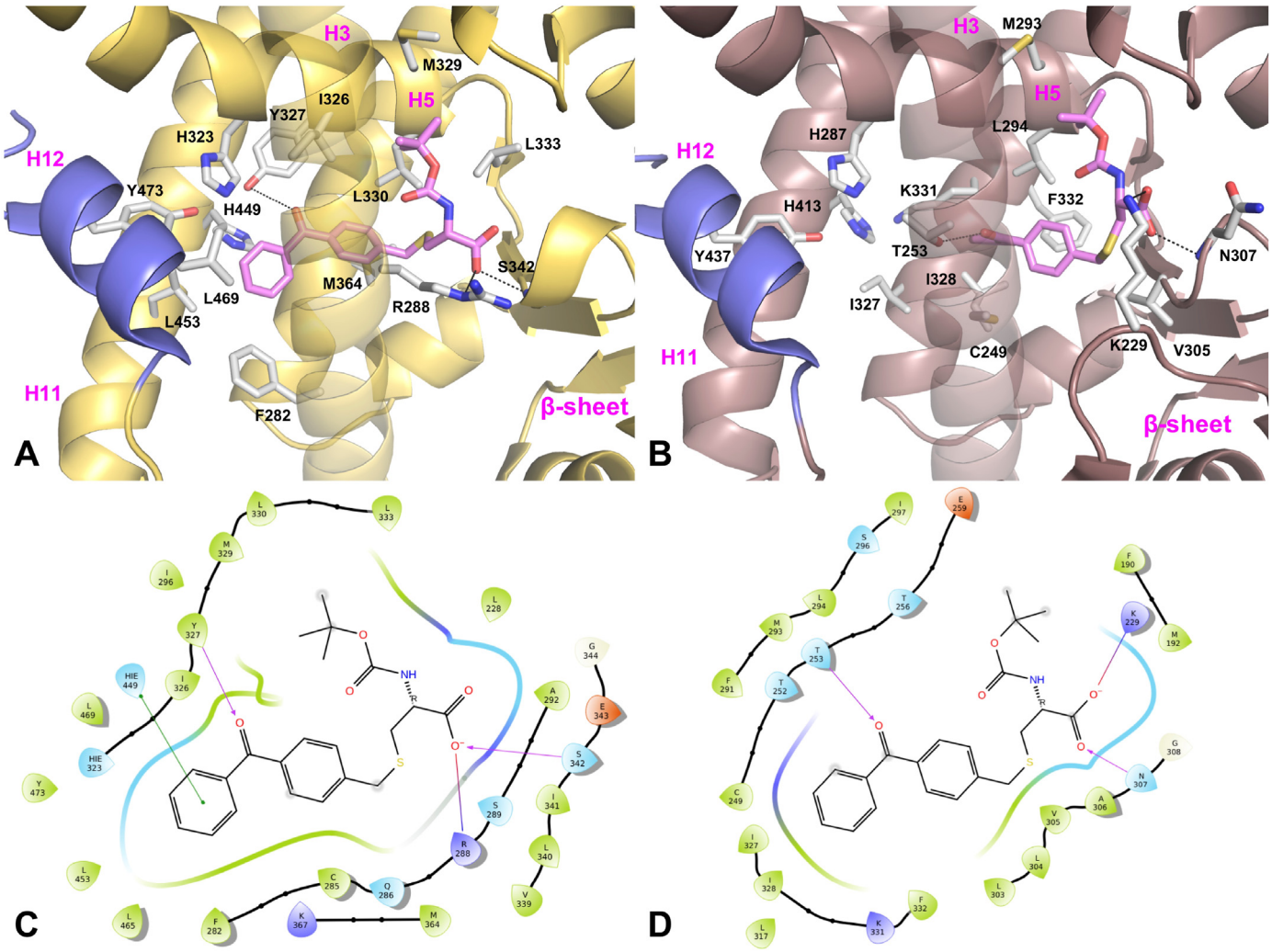

Fig. 7. Binding mode of (*R*)-**1** into PPARγ (A, yellow ribbons, PDB 4CI5) and -δ (B, dirty violet ribbons, PDB 5U3Q) LBDs. H12 is shown in slate. Only amino acids discussed in the main text are displayed (white sticks) and labeled. H-bonds discussed in the text are depicted as dashed black lines. 2D ligand interaction diagram of compound (*R*)-**1** into PPARγ (C) and -δ (D) LBDs. Positively charged amino acids are represented with dark blue drops, negatively charged amino acids are represented with red drops, polar amino acids are represented with light blue drops and hydrophobic amino acids are represented with green drops. H-bonds are depicted with purple arrows. Straight green lines represent π-stacking interactions. Straight blue-red lines represent salt bridges.

ionization (ESI). ^{1}H NMR spectra were recorded using suitable deuterated solvents on a Varian Mercury 300 NMR Spectrometer or an Agilent VNMRS500. Chemical shifts (δ) are expressed as parts per million (ppm) and the coupling constants (J) are expressed in Hertz (Hz). ^{13}C NMR (75.44 MHz) was recorded in $CDCl_3$ on a Varian Mercury 300 NMR Spectrometer for (*R*)-**1** which underwent all biological assays. Microanalyses of final compounds were carried out with a Eurovector Euro EA 3000 model analyzer; the analytical results are within ±0.4% of the theoretical values except for compound **9** whose purity was estimated as 90%. The enantiomeric excesses of the final acids (*R*)-**1** and (*S*)-**1** were determined by HPLC analysis on a Chiralcel AD column (4.6 mm i.d. × 250 mm, Daicel Chemical Industries, Ltd., Tokyo, Japan). Analytical liquid chromatography was performed on a PE chromatograph equipped with a Rheodyne 7725i model injector, a 785A model UV/vis detector, a series 200 model pump, and an NCI 900 model interface.

3.2.2. *General procedure for the synthesis of (R,S)-2-tert-butoxycarbonylamino-propanoic acids*

50 mmol of either (*R,S*)-2-amino-3-mercaptopropanoic acid or (*R,S*)-2-amino-3-hydroxypropanoic acid were dissolved in 21 mL of distilled water and then 21 mL of NaOH 2.5 N were added. The mixture was stirred at 0 °C, afterwards a solution of di-*tert*-butyl dicarbonate (51.3 mmol in 27 mL of acetone) was added dropwise. The reaction was then stirred at room temperature for 4 h. Acetone was evaporated under vacuum, the aqueous residue was acidified to pH 2 using citric acid 10% (110 mL), extracted using ethyl acetate (EtOAc, 3 x 200 mL) and the resulting organic layer was washed with water (1 x 300 mL) and brine (1 x 300 mL), dried on anhydrous Na_2SO_4, filtered and concentrated, affording the crude product.

3.2.3. ***(R,S)-2-tert-Butoxy-carbonylamino-3-mercapto-propanoic acid:*** *purified via crystallization from $CHCl_3$*

White solid, 43% yield. ^{1}H NMR (300 MHz, $CDCl_3$): δ = 6.54 (bs, 1H, COOH), 5.44 (d, J = 7.2, 1H, ex. D_2O, CH*NH*CO), 4.67–4.64 (m, 1H, CH_2*CH*COOH), 3.08–2.91 (m, 2H, *SCH*$_2$CH), 1.46 (s, 9H, (*CH*$_3$)$_3$CO). ESI-MS (abundance %, *m/z*): negative: 441 (11) [2M − 1]$^-$; 220 (45) [M − 1]$^-$; 146 (100); positive: 244 (50) [M+Na]$^+$. mp: 130–134 °C.

3.2.4. ***(R,S)-2-tert-Butoxy-carbonylamino-3-hydroxy-propanoic acid:*** *used without further purification*

Clear oil, 68% yield. ^{1}H NMR (300 MHz, $CDCl_3$): δ = 7.75 (bs, 1H, COOH), 5.89 (d, J = 7.7, 1H, ex. D_2O, CH*NH*CO), 4.34–4.31 (m, 1H, CH_2*CH*COOH), 4.04–3.81 (m, 2H, O*CH*$_2$CH), 1.40 (s, 9H, (*CH*$_3$)$_3$CO).

ESI-MS (abundance %, *m*/*z*): negative: 409 (8) $[2M - 1]^-$; 204 (88) $[M - 1]^-$; 130 (100); positive: 433 (17) $[2\ M + Na]^+$; 228 (100) $[M+Na]^+$; 172 (26); 128 (2).

3.2.5. Synthesis of (R,S)-2-benzyloxycarbonylamino-3-(2-benzyloxycarbonylamino-carboxyethyl-disulfanyl)propanoic acid

2.91 mmol of (*R*,*S*)-cystine were dissolved in water/THF (9:1, 7 mL) at room temperature. Then, NaOH 6 N was added up to pH 10, CBz-Cl was added dropwise at 0 °C and pH was finally restored to 10 using an appropriate amount of NaOH 6 N solution. The reaction was stirred at 0 °C for 3 h, after which THF was evaporated under vacuum, the solution was quenched with 12 mL distilled water and was again brought to pH 10. The aqueous layer was washed with diethyl ether (Et_2O, 2x15 mL) and acidified to pH 2 by adding HCl 1 N. The formation of a white precipitate occurred which was extracted by EtOAc (3 x 15 mL). This organic layer was washed with HCl 0.5 N (1 x 25 mL) and brine, dried over anhydrous Na_2SO_4 and filtered; then the solvent was evaporated in vacuo affording the desired compound. Pale yellow solid, 77% yield. ^{1}H NMR (500 MHz, CD_3OD): δ = 7.38–7.28 (m, 10H, aromatic), 5.11 (s, 4H, 2 O*CH*$_2$Ph), 4.53–4.50 (m, 2H, 2 CH), 3.29–3.25 and 3.02–2.96 (m, 4H, 2 *CH*$_2$CH). ESI-MS (abundance %, *m*/*z*): negative: 507 (90) $[M - 1]^-$; positive: 531 $[M+Na]^+$.

3.2.6. Synthesis of 2-benzyloxycarbonylamino-3-mercaptopropanoic acid

2.24 mmol of (*R*,*S*)-2-benzyloxycarbonylamino-3-(2-benzyloxycarbonylamino-carboxyethyl-disulfanyl)propanoic acid were dissolved in THF/water (10:1, 18 mL) at room temperature. Then P(Ph)$_3$ was added (2.46 mmol) and the mixture was stirred at room temperature for 18 h. THF was then evaporated under vacuum, 17 mL of distilled water were added, and NaOH 6 N was added up to pH 10. The aqueous layer was washed with EtOAc (1 x 15 mL) and then acidified with HCl 6 N up to pH 2. The resulting white precipitate was extracted with EtOAc (3 x 15 mL), the organic layer was separated and washed with HCl 0.5 N (1 x 40 mL) and brine (1 x 40 mL), dried over anhydrous Na_2SO_4, filtered and the solvent was evaporated to dryness affording the desired product which was purified by crystallization from $CHCl_3$/*n*-hexane. White solid, 54% yield. ^{1}H NMR (500 MHz, $CDCl_3$): δ = 7.40–7.33 (m, 5H, aromatic), 5.71 (d, J = 7.3, 1H, ex. D_2O, CH*NH*CO), 5.15 (s, 2H, Ph*CH*$_2$O), 4.75–4.72 (m, 1H, CH$_2$*CH*COOH), 4.20 (bs, 1H, COOH), 3.10–3.02 (m, 2H, S*CH*$_2$CH), 1.48 (t, J = 8.8, 1H, SH ex. D_2O). ESI-MS (*m*/*z*, abundance %): negative: 254 (34) $[M - 1]^-$; 146 (100); positive: 278 $[M+Na]^+$.

General procedure for the synthesis of 25 and 38: the appropriate benzophenones (4-bromomethyl-benzophenone or (4-bromomethyl-4′-chloro-benzophenone) were dissolved in trifluoroacetic acid under nitrogen atmosphere in a 1:4 stoichiometric ratio. Triethylsilane 97% was subsequently added in the same stoichiometric quantity as trifluoroacetic acid. The reaction mixture was then heated to 60 °C and stirred for 18 h. The mixture was cooled, dissolved in EtOAc (5 mL) and the organic layer was washed with three times with $NaHCO_{3(ss)}$ and once with brine, then it was dried over anhydrous Na_2SO_4 and filtered. Following the evaporation of the solvent in vacuo, the crude products were purified via column chromatography on silica gel (eluent *n*-hexane/ethyl acetate 99.5:0.5 to 99:1).

3.2.7. 4-Benzyl-1-bromomethyl-benzene (25): white solid, 42% yield

^{1}H NMR (300 MHz, $CDCl_3$): δ = 7.32–7.15 (m, 9H, aromatic), 4.48 (s, 2H, Ph*CH*$_2$Br), 3.97 (s, 2H, Ph*CH*$_2$Ph). GC-MS (*m*/*z*, abundance %): 260 (6) $[M]^+$, 181 (100), 165 (30).

3.2.8. 1-(Bromomethyl)-4-(4-chlorobenzyl)benzene (38): white solid, 62% yield

^{1}H NMR (500 MHz, $CDCl_3$): δ = 7.35–7.31 (m, 2H, aromatic), 7.29–7.24 (m, 2H, aromatic), 7.17–7.08 (m, 4H, aromatic), 4.49 (s, 2H, Ph*CH*$_2$Br), 3.95 (s, 2H, Ph*CH*$_2$Ph). GC-MS (*m*/*z*, abundance %): 296 (10) $[M]^+$; 215 (100); 180 (31).

General procedure for the synthesis of 4-substituted phenyl-4′-tolyl-methanones: the appropriate 4-substituted benzoyl-chloride (6 mmol), obtained by reaction of the corresponding acid with $SOCl_2$, was dissolved in toluene, and $AlCl_3$ (8.4 mmol) was added to the mixture. The reaction was stirred at room temperature for 1 h. Afterwards, cold water (2 mL) was added and the mixture was further stirred for 30 min. The resulting mixture was partitioned by water (50 mL), the organic layer was separated and further washed with $NaHCO_{3(ss)}$ (2x50 mL) and brine (1x50mL), then dried over anhydrous Na_2SO_4 and filtered. Evaporation of the solvent to dryness afforded a crude product which was purified via crystallization from *n*-hexane.

3.2.9. (4-Chloro-phenyl)-p-tolyl-methanone (32): white solid, 65% yield

^{1}H NMR (300 MHz, $CDCl_3$): δ = 7.78 (d, J = 8.8, 2H, aromatic), 7.69 (d, J = 8.0, 2H, aromatic), 7.45 (d, J = 8.8, 2H, aromatic), 7.28 (d, J = 8.3, 2H, aromatic), 2.44 (s, 3H, Ph*CH*$_3$). GC-MS (*m*/*z*, abundance %): 230 (50) $[M]^+$; 139 (28) $[C_7H_4ClO]^+$; 119 (100); 91 (23).

3.2.10. (4-Methoxy-phenyl)-p-tolyl-methanone (33): white solid, 18% yield

^{1}H NMR (300 MHz, $CDCl_3$): δ = 7.83–7.79, 7.69–7.66, 7.29–7.26, 6.99–6.93, (m, 8H, aromatic), 3.89 (s, 3H, *CH*$_3$O), 2.44 (s, 3H, Ph*CH*$_3$). ESI-MS (*m*/*z*, abundance %): positive: 249 (100) $[M+Na]^+$.

3.2.11. (4-Methyl-phenyl)-p-tolyl-methanone (34): beige solid, 42% yield

^{1}H NMR (300 MHz, $CDCl_3$): δ = 7.72–7.69, 7.29–7.26 (m, 8H, aromatic), 2.44 (s, 6H, 2(Ph*CH*$_3$). GC-MS (*m*/*z*, abundance %): 210 (51) $[M]^+$; 195 (23); 119 (100); 91 (34).

3.2.12. (4-Nitro-phenyl)-p-tolyl-methanone (35): pale yellow solid, 76% yield

^{1}H NMR (300 MHz, $CDCl_3$): δ = 8.35–8.31, 7.93–7.89, 7.72–7.70, 7.33–7.30 (m, 8H, aromatic), 2.46 (s, 3H, *CH*$_3$Ph). GC-MS (*m*/*z*, abundance %); 241 (44) $[M]^+$; 119 (100); 91 (31).

3.2.13. (4-Trifluoromethyl-phenyl)-p-tolyl-methanone (36): white solid, 45% yield

^{1}H NMR (300 MHz, $CDCl_3$): δ = 7.88–7.85, 7.76–7.70, 7.32–7.28, (m, 8H, aromatic), 2.45 (s, 3H, *CH*$_3$Ph). GC-MS (*m*/*z*, abundance %): 264 (42) $[M]^+$; 173 (11) $[C_8H_4OF_3]^+$; 145 (19); 119 (100); 91 (26).

3.2.14. Synthesis of 1-phenyl-3-p-tolyl-propenone (37)

p-tolylbenzaldehyde (16.65 mmol) was dissolved in EtOH 96°. Then, a solution of NaOH 3 M (8.4 mL) and acetophenone (16.65 mL) were added. The mixture was stirred at room temperature for 2 h, affording a yellow solid which was filtered and washed with cold distilled water. 80% yield. ^{1}H NMR (300 MHz, $CDCl_3$): 8.04–8.00 (m, 2H, aromatic), 7.80 (d, 1H, J = 15.7, CH=*CH*CO), 7.59–7.47 (m, 5H, aromatic), 7.49 (d, 1H, J = 15.7, Ph*CH* = CH), 7.26–7.22 (m, 2H, aromatic), 2.40 (s, 3H, *CH*$_3$Ph). GC-MS (*m*/*z*, abundance %): 222 (34); 207 (100).

General procedure for the preparation of 20–24 and 27: the appropriate 4′-substituted 4-methylbenzophenones (**32**–**36**) or 4-calchone derivative **37** were dissolved in CCl_4 and mixed with *N*-bromo-succinimide in a 1:1 stoichiometric ratio. Benzoyl peroxide was then added in a catalytic amount. The mixture was stirred and

heated under reflux for 7 h, then cooled to room temperature and filtered over Celite. The resulting solution was dried to dryness and the crude product was purified by column chromatography on silica gel (eluent *n*-hexane/ethyl acetate 98:2).

3.2.15. (4-Bromomethyl-phenyl)-4-chloro-phenyl-methanone (20): beige solid 35% yield

^{1}H NMR (300 MHz, $CDCl_3$): δ = 7.79–7.74 (m, 4H, aromatic), 7.53–7.45 (m, 2H, aromatic), 4.53 (s, 2H, CH_2Br). GC-MS (*m*/*z*, abundance %): 312 (3) $[M+4]^+$; 310 (14) $[M+2]^+$; 308 (8) $[M]^+$; 231 (35); 229 (100).

3.2.16. (4-Bromomethyl-phenyl)-4-methoxy-phenyl-methanone (21): pale yellow solid, 52% yield

^{1}H NMR (300 MHz, $CDCl_3$): δ = 7.84–7.81, 7.75–7.72, 7.51–7.48, 6.98–6.95 (m, 8H, aromatic), 4.54 (s, 2H, CH_2Br), 3.89 (s, 3H, CH_3O). GC-MS (*m*/*z*, abundance %): 306 (38) $[M+2]^+$; 304 (39) $[M]^+$; 225 (68); 197 (100).

3.2.17. (4-Bromomethyl-phenyl)-p-tolyl-methanone (22): white solid, 42% yield

^{1}H NMR (300 MHz, $CDCl_3$): δ = 7.78–7.70, 7.51–7.48, 7.30–7.25 (m, 8H, aromatic), 4.53 (s, 2H, PhCH_2Br), 2.44 (s, 3H, CH_3Ph). GC-MS (*m*/*z*, abundance %): 290 (16) $[M+2]^+$; 288 (16) $[M]^+$; 209 (100); 181 (95).

3.2.18. (4-Bromomethyl-phenyl)-4-nitro-phenyl-methanone (23): white solid, 40% yield

^{1}H NMR (300 MHz, $CDCl_3$): δ = 8.37–8.33, 7.95–7.91, 7.80–7.77, 7.56–7.53 (m, 8H, aromatic), 4.54 (s, 2H, BrCH_2Ph). GC-MS (*m*/*z*, abundance %): 321 (2) $[M+2]^+$, 319 (2) $[M]^+$, 241 (100).

3.2.19. (4-Bromomethyl-phenyl)-4-trifluoromethyl-phenyl-methanone (24): white solid, 27% yield

^{1}H NMR (300 MHz, $CDCl_3$): δ = 7.91–7.86, 7.80–7.72, 7.55–7.49 (m, 8H, aromatic), 4.52 (s, 2H, BrCH_2Ph). GC-MS (*m*/*z*, abundance %): 344 $[M+2]^+$ (3) 342 (3) $[M]^+$, 263 (100), 235 (55).

3.2.20. 3-(4-Bromomethyl-phenyl)-1-phenyl-propenone (27): white solid, 22% yield

^{1}H NMR (300 MHz, $CDCl_3$): δ = 8.04–8.00 (m, 2H, aromatic), 7.80 (d, 1H, J = 15.7, CH=*CH*CO), 7.64–7.43 (m, 5H, aromatic), 7.49 (d, 1H, J = 15.7, Ph*CH* = CH), 7.26–7.22 (m, 2H, aromatic), 4.51 (s, 2H, BrCH_2Ph). GC-MS (*m*/*z*, abundance %): 302 (4) $[M+2]^+$; 300 (4) $[M]^+$; 221 (100).

Synthesis of 4-chloro-4′-methyl-diphenyl (40): 4-bromotoluene (2.94 mmol), 4-chloro-benzenboronic acid (3.53 mmol), $Pd(OAc)_2$ (1 mg), TBAB 10% (95 mg), and K_2CO_3 (366 mg) were dissolved in 12 mL of PEG400. The resulting mixture was stirred at 100 °C overnight. The solution was then filtered over Celite and dissolved in EtOAc, partitioned by water, dried over anhydrous Na_2SO_4 and evaporated in vacuo, affording the crude product as a white solid which was purified by crystallization from $CHCl_3$/*n*-hexane. White solid, 75% yield. ^{1}H NMR (500 MHz, $CDCl_3$): δ = 7.52–7.50, 7.47–7.45, 7.41–7.39, 7.27–7.25 (m, 8H, aromatic), 2.41 (s, 3H, PhCH_3). GC-MS (*m*/*z*, abundance %): 204 (33) $[M+2]^+$; 202 (100) $[M]^+$; 165 (50); 152 (18).

*3.2.21. Synthesis of 4′-bromomethyl-4-chloro-diphenyl (39): compound **40** (2.20 mmol) was dissolved in CCl_4 (30 mL) and the mixture was stirred at room temperature*

N-bromo-succinimide (2.20 mmol) and benzoyl peroxide (catalytic amount) were added. The reaction mixture was refluxed overnight, then cooled at room temperature and the suspension was filtered over Celite. The resulting filtrate was evaporated to dryness and purified via column chromatography on silica gel (eluent: *n*-hexane). Pale yellow solid, 45% yield. ^{1}H NMR (500 MHz, $CDCl_3$): δ = 7.54–7.49, 7.43–7.41 (m, 8H, aromatic), 4.56 (s, 2H, PhCH_2Br). GC-MS (*m*/*z*, abundance %): 284 (2) $[M+4]^+$; 282 (6) $[M+2]^+$; 280 (5) $[M]^+$; 203 (33); 201 (100).

3.2.22. General procedure for the preparation of target acids 1–3, 7, 8, 10–12, 17, 18

NaH (6 eq) was suspended in dry DMF, then the appropriate *tert*-butoxy- or benzyloxy-carbonylamino-propanoic acids (1.1 eq) and bromides (1 eq), dissolved in anhydrous DMF, were added dropwise under inert atmosphere at 0 °C. The reaction mixture was stirred at room temperature for 24 h, then quenched by ice and HCl 2 N up to pH 2. The resulting aqueous solution was extracted using EtOAc, and the organic phase was washed with distilled water and brine, dried over anhydrous Na_2SO_4, filtered and evaporated in vacuo. Some of the desired acids were purified as benzylamine or cyclohexylamine salts.

3.2.23. (R,S)-3-(4-Benzoyl-benzylsulfanyl)-2-tert-butoxycarbonylamino-propanoic acid, benzylamine salt (1): pale yellow solid, 43% yield

^{1}H NMR (300 MHz, $CDCl_3$): δ = 7.78–7.70, 7.60–7.56, 7.49–7.30 (m, 14H, aromatic), 5.46–5.43 (m, 1H, ex. H_2O, CH*NH*CO), 4.21–4.19 (m, 1H, CH_2*CH*COO), 3.98 (s, 2H, Ph$CH_2NH_3^+$), 3.74 (s, 2H, PhCH_2S), 2.91–2.74 (m, 2H, SCH_2CH), 1.42 (s, 9H, $(CH_3)_3$CO). ESI-MS (*m*/*z*, abundance %): negative: 414 (100) $[M-1]^-$; 340 (20); 296 (10). Elemental analysis: calculated ($C_{28}H_{34}N_2O_5S\cdot 0.5H_2O$) C: 65.51%; H: 6.64%; N: 5.27%; found C: 65.95%; H: 6.42%; N: 5.45%.

*3.2.24. (R)-3-(4-Benzoyl-benzylsulfanyl)-2-tert-butoxycarbonylamino-propanoic acid, benzylamine salt ((R)-1): this enantiomer was prepared starting from Boc-L-cysteine and **19***

^{13}C NMR: 28.4, 34.4, 36.6, 43.6, 55.2, 79.5, 128.2–137.6, 143.4, 155.5, 176.2, 196.2. The free acid was analyzed by HPLC (Chiralcel AD column, flux 1 mL/min, λ = 254 nm, n-hexane/isopropanol/trifluoroacetic acid 80/20/0.2, Rt = 23.96 min): e.e. ≥ 98%.

(*S*)-3-(4-Benzoyl-benzylsulfanyl)-2-*tert*-butoxycarbonylamino-propanoic acid, benzylamine salt ((*S*)-1): this enantiomer was prepared starting from Boc-D-cysteine and **19**; the free acid was analyzed by HPLC (Chiralcel AD column, flux 1 mL/min, λ = 254 nm, n-hexane/isopropanol/trifluoroacetic acid 80/20/0.2, Rt = 12.10 min): e.e. ≥ 98%.

3.2.25. (R,S)-2-tert-Butoxycarbonylamino-3-[4-(4-chloro-benzoyl) benzylsulfanyl]propanoic acid, benzylamine salt (2): white solid, 19% yield

^{1}H NMR (300 MHz, $CDCl_3$): δ = 7.72–7.66, 7.45–7.27 (m, 13H, aromatic), 5.52–5.49 (m, 1H, ex. H_2O, CH*NH*CO), 4.16–4.14 (m, 1H, CH_2*CH*COO^-), 3.96 (s, 2H, Ph$CH_2NH_3^+$), 3.73 (s, 2H, PhCH_2S), 3.48–3.33 (bs, ex. H_2O, Ph$CH_2NH_3^+$), 2.90–2.72 (m, 2H, SCH_2CH), 1.42 (s, 9H, $(CH_3)_3$CO). ESI-MS (*m*/*z*, abundance %): negative: 450 $[M+2-H]^-$ 448 (100) $[M-H]^-$; 374 (14); 330 (8). Elemental analysis ($C_{29}H_{33}ClN_2O_5S\cdot H_2O$): calculated: C: 60.56%; H: 6.13%; N: 4.87%; found: C: 60.85%; H:5.84%; N: 5.16%.

3.2.26. (R,S)-2-tert-Butoxycarbonylamino-3-[4-(4-methoxy-benzoyl)-benzylsulfanyl]-propanoic acid, benzylamine salt (3): white solid, 42% yield

^{1}H NMR (300 MHz, $CDCl_3$): δ = 7.81–7.77, 7.66–7.64, 7.39–7.24, 6.96–6.92 (m, 13H, aromatic), 5.52–5.49 (m, 1H, ex. H_2O, NH), 4.15–4.13 (m, 1H, *CH*CH_2) 3.96 (s, 2H, Ph$CH_2NH_3^+$), 3.88 (s, 3H, CH_3O), 3.72 (s, 2H, PhCH_2S), 3.63 (bs, 3H, NH_3^+), 2.87–2.71 (m, 2H, SCH_2CH), 1.42 (s, 9H, $(CH_3)_3$CO). ESI-MS (*m*/*z*, abundance %): negative: 444 (38) $[M-H]^-$; 370 (18); 326 (7); 257 (100). Elemental

analysis ($C_{30}H_{36}N_2O_6S\cdot0.5H_2O$): calculated: C: 64.15%; H: 6.64%; N: 4.99%; found: C: 64.40%; H: 6.44%; N: 5.31%.

3.2.27. (R,S)-3-(4-Benzyl-benzylsulfanyl)-2-tert-butoxycarbonylamino-propanoic acid, benzylamine salt (7): white solid, 56% yield

^{1}H NMR (300 MHz, $CDCl_3$): δ = 8.08 (s, 1H, NH) 7.33–7.06 (m, 14H, aromatic), 5.47 (d, J = 6.3, 1H, ex. H_2O, CH*NH*CO), 4.11 (d, J = 5.2, 1H, CH_2*CH*CO), 3.91 (s, 4H, Ph*CH*$_2$Ph and Ph*CH*$_2$$NH_3^+$), 3.62 (s, 2H, Ph*CH*$_2$S), 2.81–2.67 (m, 2H, S*CH*$_2$CH), 1.41 (s, 9H, $(CH_3)_3$CO). ESI-MS (*m*/*z*, abundance %): negative: 400 (84) $[M-1]^-$; 326 (31); 213 (34); positive: 424 (54) $[M+Na]^+$ 368 (100); 324 (58). Elemental analysis ($C_{29}H_{36}N_2O_4S\cdot1.5H_2O$): calculated: C: 65.02%; H: 7.34%; N: 5.23%; found: C: 65.26%; H: 6.85%; N: 5.52%.

3.2.28. (R,S)-3-(Diphenyl-4-ylmethylsulfanyl)-2-tert-butoxy-carbonyl-amino-propanoic acid (8): white solid. 93% yield

^{1}H NMR (300 MHz, $CDCl_3$): δ = 7.61–7.53, 7.46–7.40, 7.37–7.31 (m, 9H, aromatic), 5.32–5.29 (m, 1H, ex. H_2O, CH*NH*CO), 4.52–4.47 (m, 1H, CH_2*CH*COOH), 3.80 (s, 2H, Ph*CH*$_2$S), 2.95–2.10 (m, 2H, S*CH*$_2$CH), 1.46 (s, 9H, $(CH_3)_3$CO). ESI-MS (*m*/*z*, abundance %): negative: 773 (14) $[2M-H]^-$; 386 (100); 312 (37); 199 (50). Elemental analysis($C_{21}H_{25}NO_4S\cdot0.5H_2O$): calculated: C: 63.61%; H: 6.61%; N: 3.53%, found C: 63.81%; H:6.57%; N: 3.62%. mp: 133–134 °C.

3.2.29. (R,S)-3-(4-Benzoyl-benzyloxy)-2-tert-butoxycarbonylamino-propanoic acid, cyclohexylamine salt (10): white solid, 60% yield

^{1}H NMR (300 MHz, $CDCl_3$): δ = 7.77–7.40 (m, 9H, aromatic), 5.58–5.55 (m, 1H, CH*NH*CO), 4.61 (s, 2H, PH*CH*$_2$O), 4.14–3.79 (m, 3H, *CHCH*$_2$), 2.99–2.90 (m, 1H, cyclohexylamine CH), 2.02–1.98, 1.75–1.16 (m, 10H, cyclohexylamine $(CH_2)_5$), 1.42 (s, 9H, $(CH_3)_3$CO). ESI-MS (*m*/*z*, abundance %): negative: 398 (100) $[M-1]^-$; 324 (55); 211 (60); positive: 422 (100) $[M+Na]^+$; 366 (24); 322 (15). Elemental analysis: calculated ($C_{28}H_{38}N_2O_6\cdot1.5H_2O$): C: 63.98%; H: 7.86%; N: 5.33%; found: C: 63.76%; H: 7.44%; N: 5.35%.

3.2.30. (R,S)-3-(4-Benzyl-benzyloxy)-2-tert-butoxy-carbonylamino-propanoic acid, benzylamine salt (11): white solid, 62% yield

^{1}H NMR (300 MHz, $CDCl_3$): δ = 7.36–7.06 (m, 14H, aromatic), 6.46 (bs, 3H, ex. H_2O, PhCH*NH*$_3^+$), 5.48–5.45 (m, 1H, CH*NH*CO), 4.34 (s, 2H, O*CH*$_2$Ph), 4.04–3.98 (m, 1H, CH_2*CH*COO^-), 3.89 (s, 2H, Ph*CH*$_2$Ph), 3.74 (s, 2H, Ph*CH*$_2$$NH_3^+$), 3.69–3.60 (m, 2H, O*CH*$_2$CH), 1.39 (s, 9H, $(CH_3)_3$CO). ESI-MS (*m*/*z*, abundance %): negative: 769 (17) $[2M-1]^-$; 384 (100) $[M-1]^-$; 310 (71); 196 (20). Elemental analysis: calculated ($C_{29}H_{36}N_2O_5$): C: 70.71%; H: 7.31%; N: 5.69%; C: 70.24%; H: 7.27%; N: 5.70%.

3.2.31. (R,S)-3-(Biphenyl-4-ylmethoxy)-2-tert-butoxy-carbonylamino-propanoic acid, benzylamine salt (12): white solid, 19% yield

^{1}H NMR (300 MHz, $CDCl_3$): δ = 7.53–7.29 (m, 14H, aromatic), 5.85 (bs, 1H, CH*NH*COO^-), 5.53 (bs, 3H, $PhCH_2$*NH*$_3^+$), 4.45 (s, 2H, Ph*CH*$_2$O), 4.10–4.05 (m, 1H, CH_2*CH*COO^-), 3.92–3.63 (m, 2H, *CH*$_2$CH), 3.85 (s, 2H, Ph*CH*$_2$$NH_3^+$), 1.40 (s, 9H, $(CH_3)_3$CO). ESI-MS (*m*/*z*, abundance %): negative: 370 (22) $[M-1]^-$; 296 (18); 183 (10). Elemental analysis: calculated: 70.27%; H: 7.16%; N: 5.85%; found: C: 69.96%; H:6.95%; N: 5.66%.

3.2.32. (R,S)-2-Benzyloxycarbonylamino-3-[4-(4-chloro-benzyl)-benzylsulfanyl]propanoic acid, benzylamine salt (17): pale yellow solid, 28% yield

^{1}H NMR (500 MHz, $CDCl_3$): δ = 7.37–7.34, 7.26–7.24, 7.10–7.07 (m, 18H, aromatic), 5.55–5.52 (m, 1H, CH*NH*Cbz), 5.12 (s, 2H, Ph*CH*$_2$O), 4.51 (s, 2H, Ph*CH*$_2$Ph), 3.90 (m, 1H, CH_2*CH*COO^-), 3.80 (s, 2H, Ph*CH*$_2$$NH_3^+$), 3.70 (s, 2H, Ph*CH*$_2$S), 2.95–2.85 (m, 2H, S*CH*$_2$CH). ESI-MS (*m*/*z*, abundance %): negative: 468 (65) $[M-1]^-$; 360 (4). Elemental analysis ($C_{32}H_{33}ClN_2O_4S\cdot H_2O$): calculated: C: 64.58%, H: 5.93%, N: 4.71%; C: 64.53%, H: 5.66%, N: 5.17%.

3.2.33. (R,S)-2-Benzyloxycarbonylamino-3-(4′-chloro-diphenyl-4-ylmethylsulfanyl)propanoic acid, benzylamine salt (18): white solid, 23% yield

^{1}H NMR (300 MHz, $CDCl_3$): δ = 7.58–7.31 (m, 18H, aromatic), 5.56–5.54 (d, J = 6.8, 1H, CH*NH*CO), 5.13 (s, 2H, Ph*CH*$_2$O), 4.60–4.62 (m, 1H, CH_2*CH*COOH), 4.51 (s, 2H Ph*CH*$_2$S), 3.77 (s, 2H, Ph*CH*$_2$$NH_3^+$), 3.03–2.92 (m, 2H, S*CH*$_2$CH), 2.38 (bs, 3H, *NH*$_3^+$). ESI-MS (*m*/*z*, abundance %): negative: 454 (6) $[M-H]^-$; 346 (30); 233 (100) $[C_{13}H_{10}SCl]^-$. Elemental analysis ($C_{31}H_{31}ClN_2O_4S\cdot1.5H_2O$): calculated: C: 63.09%, H: 5.81%, N: 4.75%; found C: 63.20%, H: 5.36%, N: 4.93%.

3.2.34. General procedure for the preparation of 28–31 and 13

(*R*,*S*)-cysteine was dissolved in a solution of NaOH 2 N/EtOH (2mL/0.5 mL) and mixed with the appropriate ketone in a 0.9:1 stoichiometric ratio. The resulting mixture was stirred at room temperature for 30 min. The reaction was then cooled to 0 °C and HCl 2 N was added up to pH 6–7, causing the formation of a precipitate. This precipitate was filtered, washed with distilled water, EtOH and Et_2O, and crystallized from H_2O. The crystals were washed with EtOH, affording the desired products as white solids.

3.2.35. (R,S)-2-Amino-3-[4-(4-methyl-benzoyl)-benzylsulfanyl] propanoic acid (28): 34% yield

^{1}H NMR (300 MHz, DMSO-d_6): δ = 7.67–7.61, 7.53–7.50, 7.36–7.34 (m, 8H, aromatic), 3.90–3.79 (m, 1H, CH_2*CH*), 3.49 (s, 2H, *CH*$_2$S) 2.94–2.66 (m, 2H, S*CH*$_2$CH), 2.39 (s, 3H, *CH*$_3$Ph). ESI-MS (*m*/*z*, abundance %): negative: 328 (31) $[M-1]^-$; 241 (100).

3.2.36. (R,S)-2-Amino-3-[4-(4-nitro-benzoyl)-benzylsulfanyl] propanoic acid (29): 35% yield

^{1}H NMR (300 MHz, DMSO-d_6): δ = 8.38–8.35, 7.95–7.92, 7.74–7.72, 7.58–7.55 (m, 8H, aromatic), 3.92–3.80 (m, 1H, CH_2*CH*COOH), 3.48 (s, 2H, *CH*$_2$S) 2.93–2.68 (m, 2H, S*CH*$_2$CH). ESI-MS (*m*/*z*, abundance %): negative: 719 (18) $[2M-H]^-$; 359 (98) $[M-H]^-$; 271 (100).

3.2.37. (R,S)-2-Amino-3-[4-(4-trifluoromethyl-benzoyl)-benzylsulfanyl]propanoic acid (30): 75% yield

ESI-MS (*m*/*z*, abundance %): negative: 382 (100) $[M-1]^-$.

3.2.38. (R,S)-2-Amino-3-[4-(3-oxo-phenyl-propenyl)-benzylsulfanyl]propanoic acid (31): 43% yield

ESI-MS (*m*/*z*, abundance %): negative: 340 (100) $[M-H]^-$, 253 (99).

3.2.39. (R,S)-2-amino-3-(4-benzoyl-benzylsulfanyl)-propanoic acid (13): 13% yield

^{1}H NMR (300 MHz, DMSO-d_6): δ = 7.73–7.64, 7.57–7.52 (m, 9H, aromatic), 3.91–3.80 (m, 1H, CH_2*CH*), 3.49 (s, 2H, Ph*CH*$_2$) 2.94–2.66 (m, 2H, S*CH*$_2$CH). ESI-MS (*m*/*z*, abundance %): negative: 314 (90) $[M-H]^-$; 227 (100). Elemental analysis ($C_{17}H_{17}NO_3S$): calculated: C:64.74%, H:5.43%, N:4.44%; found: C:64.27%, H: 5.41%, N: 4.53%. mp: 168–170 °C.

General procedure for the preparation of 4–6 and 9: the appropriately substituted 2-amino-3-benzylsulfanyl propanoic acid was dissolved in H_2O/dioxane 1:1 solution and mixed with triethylamine and Boc_2O in a 1:1.8:1 stoichiometric ratio. The

reaction mixture was stirred at room temperature for 4 h in the dark. The solvent was subsequently removed in vacuo and HCl was added up to pH 1. The aqueous solution was extracted three times by EtOAc, and the organic phase was washed once with brine, dried over anhydrous Na_2SO_4, filtered and the evaporated to dryness, affording the crude product which was subjected to further purification via salt formation with benzylamine or via crystallization.

3.2.40. (R,S)-2-tert-Butoxycarbonylamino-3-[4-(4-methyl-benzoyl)-benzylsulfanyl]propanoic acid, benzylamine salt (4): 82% yield

^{1}H NMR (300 MHz, $CDCl_3$): δ = 7.69–7.66, 7.38–7.21 (m, 13H, aromatic), 5.54–5.52 (m, 1H, ex. H_2O, CH*NH*CO), 4.17–4.12 (m, 1H, CH_2*CH*COO^-), 3.94 (s, 2H, Ph*CH*$_2$$NH_3^+$), 3.73 (s, 2H, Ph*CH*$_2$S), 3.36 (bs, 3H, NH_3^+), 2.88–2.74 (m, 2H, S*CH*$_2$CH), 2.46 (s, 3H, CH_3Ph), 1.42 (s, 9H, $(CH_3)_3$CO). ESI-MS (*m*/*z*, abundance %): negative: 428 (100) [M – 1]$^-$; 354 (25); 310 (4). Elemental analysis ($C_{30}H_{36}N_2O_5S\cdot0.5H_2O$): calculated: C:66.03%; H:6.83%; N:5.13%; found: C:65.70%; H:6.65%; N: 5.08%.

3.2.41. (R,S)-2-tert-Butoxycarbonylamino-3-[4-(4-nitro-benzoyl)-benzylsulfanyl]propanoic acid, benzylamine salt (5): 99% yield

^{1}H NMR (300 MHz, DMSO-d_6): δ = 8.36–8.33, 7.94–7.91, 7.71–7.68, 7.51–7.48, 7.49–7.29 (m, 13H, aromatic), 6.29–6.27 (m, 1H, ex. H_2O, CH*NH*CO), 3.92 (s, 2H, Ph*CH*$_2$$NH_3^+$), 3.92–3.80 (m, 6H, *CH*, S*CH*$_2$, NH_3^+), 2.85–2.69 (m 2H, *CH*$_2$CH), 1.36 (s, 9H, $(CH_3)_3$CO). ESI-MS (*m*/*z*, abundance %): negative: 459 (100) [M – H]$^-$; 385 (4); 341 (6). Elemental analysis ($C_{29}H_{35}N_3O_8S\cdot H_2O$): C, 59.47; H, 6.02; N, 7.17; found: C:59.63; H:5.76; N:7.26%.

3.2.42. (R,S)-2-tert-Butoxycarbonylamino-3-[4-(4-trifluoromethyl-benzoyl)benzylsulfanyl]-propanoic acid (6): the crude product was purified via crystallization from $CHCl_3$/n-hexane. 55% yield

^{1}H NMR (300 MHz, $CDCl_3$): δ = 7.90–7.87, 7.77–7.74, 7.47–7.44 (m, 8H, aromatic), 5.34–5.31 (m, 1H, ex. H_2O, CH*NH*CO), 4.56–4.52 (m, 1H, CH_2*CH*COOH), 3.82 (s, 2H, Ph*CH*$_2$S), 3.02–2.82 (m, 2H, S*CH*$_2$CH), 1.45 (s, 9H, $(CH_3)_3$CO). ESI-MS (*m*/*z*, abundance %): negative: 482 (100) [M – H]$^-$. Elemental analysis ($C_{23}H_{24}F_3NO_5S\cdot0.5H_2O$): C:56.09%; H:5.12%; N:2.84%; found: C:56.40%; H:4.97%; N: 2.93%. mp: 120–124 °C.

3.2.43. (R,S)-2-tert-butoxycarbonylamino-3-[4-(3-oxo-3-phenyl-propenyl)benzylsulfanyl]-propanoic acid, benzylamine salt (9): 75% yield

^{1}H NMR (300 MHz, $CDCl_3$): δ = 8.02–7.99 (m, 2H, aromatic), 7.77 (d, J = 15.7, 1H, CO*CH*=CH), 7.60–7.47 (m, 7H, 6 aromatic and CH=*CH*Ph), 7.38–7.27 (m, 6H, aromatic), 5.41–5.38 (m, 1H, ex. H_2O, CH*NH*CO), 4.46–4.29 (m, 1H, CH_2*CH*COOH) 4.02 (s, 2H, Ph*CH*$_2$$NH_3^+$), 3.74 (s, 2H, Ph*CH*$_2$S), 2.94–2.77 (m, 2H, S*CH*$_2$CH), 1.43 (s, 9H, $(CH_3)_3$CO). ESI-MS (*m*/*z*, abundance %): negative: 440 (100) [M – 1]$^-$ 366 (15); 322 (5); 253 (23).

Synthesis of the benzylamine salt of (*R,S*)-2-acetylamino-3-(4-benzoyl-benzylsulfanyl)propanoic acid (14): 2-amino-3-(4-benzoyl-benzylsulfanyl)propanoic acid (0.49 mmol) was added to a 1:1 water/dioxane mixture (3 mL). The reaction was stirred at 0 °C and a solution of NaOH 2 N (0.20 mL) was added. To the resulting solution was added dropwise simultaneously a solution of acetyl chloride (0.51 mmol) in dioxane (0.4 mL) and an aqueous solution of NaOH 1 N (0.4 mL). The mixture was stirred at room temperature for 30 min, then diluted with water (4 mL), and HCl was added up to pH 2. The aqueous layer was evaporated to dryness affording a white solid which was washed with water and dissolved in EtOH. The solvent was evaporated to dryness affording a crude product which was purified as benzylamine salt. 27% yield. ^{1}H NMR (300 MHz, $CDCl_3$): δ = 7.79–7.34 (m, 14H, aromatic), 6.74–6.72 (m, 1H, ex. H_2O, CH*NH*CO), 4.57–4.53 (m, 1H, CH_2*CH*COOH), 3.93 (s, 2H, Ph*CH*$_2$$NH_3^+$), 3.69 (s, 2H, Ph*CH*$_2$S), 3.47 (bs, 3H, NH_3^+), 2.87–2.74 (m, 2H, S*CH*$_2$CH), 1.87 (s, 3H, *CH*$_3$CO). ESI-MS (*m*/*z*, abundance %): negative: 356 (100) [M – H]$^-$, 227 (90). Elemental analysis ($C_{26}H_{28}N_2O_4S\cdot H_2O$): C: 64.71%, H: 6.27%, N:5.81%; found: C:65.20%, H: 6.46%, N: 5.98.

3.2.44. General procedure for the preparation of 15 and 16

(*R*,*S*)-2-Amino-3-(4-benzoyl-benzylsulfanyl)propanoic acid (0.62 mmol) was added to a solution of NaOH 2 N (4.5 mL). The mixture was stirred at 0 °C and the benzyl chloroformate or benzoylchloride was added dropwise in a 1:1.13 stoichiometric ratio. The reaction was stirred at 0 °C for 5 h, then the organic layer was washed with Et_2O and acidified adding HCl 2 N up to pH 2–3. The water layer was extracted whit EtOAc (3x20mL). The organic layer was washed with distilled water (1x40mL), brine (1x40mL), dried over Na_2SO_4, filtered and evaporated to dryness affording a solid purified by crystallization from chloroform/*n*-hexane.

3.2.45. (R,S)-2-benzoylamino-3-(4-benzoyl-benzylsulfanyl) propanoic acid (15): 66% yield

^{1}H NMR (300 MHz, DMSO-d_6): δ = 8.72 (d, J = 8.0, 1H, CH*NH*CO), 7.88–7.85, 7.72–7.44 (m, 14H, aromatic), 4.60–4.53 (m, 1H, CH_2*CH*COOH), 3.88 (s, 2H, Ph*CH*$_2$S), 3.00–2.83 (m, 2H, S*CH*$_2$CH). ESI-MS (*m*/*z*, abundance %): negative: 418 (100) [M – 1]$^-$; 227 (49); 146 (7). Elemental analysis ($C_{24}H_{21}NO_4S\cdot2/3H_2O$) calculated: 66.80%, H: 5.22%, N:3.25%; found: C:66.67%, H:4.92%, N: 3.26%. mp: 150–153 °C.

3.2.46. (R,S)-3-(4-benzoyl-benzylsulfanyl)-2-benzyloxycarbonylamino-propanoic acid (16): 42% yield

^{1}H NMR (300 MHz, $CDCl_3$): δ = 7.79–7.72, 7.61–7.57, 7.50–7.29 (m, 14H, aromatic), 5.62–5.59 (m, 1H, *NH*), 5.12 (s, 2H, Ph*CH*$_2$O), 4.63–4.58 (m, 1H, CH_2*CH*COOH), 3.78 (s, 2H, Ph*CH*$_2$*S*), 2.98–2.85 (m, 2H, S*CH*$_2$CH). ESI-MS (abundance %, *m*/*z*): negative: 448 (100) [M – 1]$^-$; 340 (66); 296 (15). Elemental analysis ($C_{25}H_{25}NO_3S$) C: 64.22%, H: 5.39%, N: 3.00%; found C:64.66%, H: 5.04%, N: 3.04%. mp: 134–136 °C.

3.3. Biological methods

3.3.1. Plasmids

The expression vectors expressing the chimeric receptor containing the yeast Gal4-DNA binding domain fused to the human PPARα, PPARγ, or PPARδ ligand binding domain (LBD) and the reporter plasmid for these Gal4 chimeric receptors (pGal5TKpGL3) containing five repeats of the Gal4 response elements upstream of a minimal thymidine kinase promoter that is adjacent to the luciferase gene were described previously [45].

3.3.2. HepG2 cells cultures and transfections

Human hepatoblastoma cell line HepG2 (Interlab Cell Line Collection, Genoa, Italy) was cultured in minimum essential medium containing 10% heat-inactivated foetal bovine serum, 100 U of penicillin G/mL, and 100 μ g of streptomycin sulfate/mL at 37 °C in a humidified atmosphere of 5% CO_2. For transactivation assays, 10^5 cells per well were seeded in a 24-well plate and transfections were performed after 24 h with CAPHOS, a calcium phosphate method, according to the manufacturer's guidelines. Cells were transfected with expression plasmids encoding the fusion protein Gal4-PPARα -LBD, Gal4-PPARγ -LBD or.

Gal4-PPARδ -LBD (30 ng), pGal5TKpGL3 (100 ng), and pCMVβ gal (250 ng). Four hours after transfection, cells were treated for 20 h with the ligands and reference compounds in duplicate. Luciferase activity in cell extracts was determined by a

luminometer (VICTOR^3 V Multilabel Plate Reader, PerkinElmer). β-Galactosidase activity was determined using ortho-nitro-phenyl-β-D-galactopyranoside as described previously [46]. All transfection experiments were repeated at least twice.

3.3.3. HepaRG cell cultures

HepaRG cells were kindly provided by Prof. Youssef Daali, University of Geneva and were used for experiments between passage 17 and 19. Cells were maintained in Williams'E with Glutamax supplemented with 10% foetal calf serum, 100U/mL penicillin, 100 μg/mL streptomycin, 5 μg/mL insulin (Sigma), and 50 μM of hydrocortisone hemisuccinate (Sigma). For experiments cells were plated in 24 well plates at a density of 2.6x10^4 cells/cm^2. After 2 weeks, 2% DMSO was added to the culture medium for two additional weeks. The obtained cells are a mixture of hepatocyte-like cells and progenitors/primitive biliary-like cells [47]. After 2 weeks cells were treated with ligands and/or oleic acid in medium for differentiation (with FBS) for the indicated time. All ligands and oleic acid were dissolved in DMSO. Oleic acid, fenofibrate were from Sigma, while rosiglitazone was from Cayman Chemicals. At the used concentrations/conditions none of the ligands were toxic (data not shown).

3.3.4. RNA extraction and real-time qPCR

Total RNA was extracted from HepaRG cells with Trizol® Reagent (Life Technologies) followed by Direct-zol™ RNA Miniprep (Zymo Research), according to manufacturer's instructions. Purified total RNA samples were quantified with Qubit fluorometer. 1 μg of total RNA was used retrotranscription with ImProm-II™ Reverse Transcription System (Promega) and the quantification of mRNA levels of PPAR target genes was done by real-time qPCR using Kapa SYBR green fast (Kapa Biosystems) in a StepOnePlus™ Real-Time PCR. RPS13 was used as housekeeping gene for data normalization.

3.3.5. Lipid Accumulation

Lipid accumulation was determined by staining cellular lipids with 0.5% Oil Red O (Sigma). Pictures were taken with a microscope Nikon Eclipse TS100 at 200X magnification. The quantification of the intracellular dye was performed after isopropanol extraction and spectrophotometric reading at 490 nm with Infinite M Nano (Tecan) spectrophotometer.

3.3.6. Statistical Analyses

Statistical analyses were performed via one-way ANOVA analysis of variance with Dunnet post-test analysis for multiple group comparisons using GraphPad Prism version 8.3.0 (GraphPad Software, San Diego, CA). Differences with p values of less than 0.05 were considered statistically significant.

3.3.7. C2C12 cell cultures and glucose uptake assay

C2C12 cells were purchased from European Collection of Authenticated Cell Cultures (ECACC). Cells were routinely grown in Dulbecco's Modified Eagle's medium (DMEM) supplemented with 10% foetal bovine serum (FBS), 2 mM glutamine, 100 IU/mL penicillin, 100 μg/mL streptomycin (Sigma-Aldrich, St. Louis, MO, USA.

To evaluate glucose uptake, C2C12 cells were plated in P35 dishes and grown until 80% confluence was achieved. Then, cells were incubated in the presence of starvation medium containing rosiglitazone (10 μM) and (R)-**1** (25 μM). Treatment was repeated for 4 days, and treatment medium was replaced every 24 h with fresh medium. After 96 h, cells were stimulated with 10 nM insulin (Humalog Lispro, Eli Lilly) for 30 min. After stimulation, cells were incubated in the presence of 40 μM of 2-NBDG (Invitrogen) for 3 h. Then, cells were washed with PBS, tripsinized, pelleted by centrifugation (1000×*g* for 5 min), then suspended in 500 μL of PBS before analysis. The amount of 2-NBDG uploaded by cells was determined analyzing cells by using a flow cytometer apparatus (FACSCanto II, BD Biosciences, San Jose, CA, USA). For each samples 1x10^4 events were acquired. Data obtained were then analyzed with FlowJo software. Cells autofluorescence values were determined before sample analysis and subtracted to each sample.

GLUT4 expression level in C2C12 cells. Murine myoblasts were treated with rosiglitazone (10 μM) and (*R*)-1 (25 μM) for 96 h in starvation medium. Every 24 h, the treatment medium was renewed. After 96 h, the cells were lysed by adding 100 μL of 1X Laemmli sample buffer solution. The expression level of GLUT4 was evaluated by Western blot analysis, probing the PVDF membrane obtained with antibodies specific for GLUT4 glucose transporter (GLUT4, clone 1F8, Mouse mAb, Cell Signaling Technology, Danvers, Massachusetts, USA). Each test was performed in triplicate. Ctr: Control test. The data shown in the figure represent the mean value ± SD (n = 3).

Author contributions

F.L. and A.L. (A. Lavecchia) designed and wrote the manuscript. A.L. (A. Laghezza), L.B., A.T. and M.G. performed pharmacological experiments. S.S. and L.P. synthesized novel compounds. C.C. and A.L. (A. Lavecchia) performed the docking simulation study. R.L. and A.S. supported chemical synthesis and analytical experiments. F.G. and P.P. reviewed the manuscript. P.T. and F.L found the resources. S.S. and C.C. contributed equally to this work. All authors have given approval to the final version of the manuscript.

Declaration of competing interest

The authors declare that they have no known competing financial interests or personal relationships that could have appeared to influence the work reported in this paper.

Acknowledgments

This work was accomplished thanks to the financial support of the Università degli Studi di Bari "Aldo Moro".

Supporting Information

Compounds identified by chemoinformatics search (Table S1); overlays of (*R*)-**1** and (*S*)-**1** docked poses (Fig. S1); In Silico ADMET Assessment (Table S2); Flow chart of the chemoinformatic approach (Fig. S2).

Appendix A. Supplementary data

Supplementary data to this article can be found online at https://doi.org/10.1016/j.ejmech.2022.114240.

References

[1] A.S. Laganà, S.G. Vitale, A. Nigro, V. Sofo, F.M. Salmeri, P. Rossetti, A.M.C. Rapisarda, S. La Vignera, R.A. Condorelli, G. Rizzo, M. Buscema, Pleiotropic actions of peroxisome proliferator-activated receptors (PPARs) in dysregulated metabolic homeostasis, inflammation and cancer: current evidence and future perspectives, Int. J. Mol. Sci. 17 (2016) 999.
[2] G.S. Harmon, M.T. Lam, C.K. Glass, PPARs and lipid ligands in inflammation and metabolism, Chem. Rev. 111 (2011) 6321–6340.
[3] A. Zieleniak, M. Wójcik, L.A. Woźniak, Structure and physiological functions of the human peroxisome proliferator-activated receptor γ, Arch. Immunol. Ther. Exp. 56 (2008) 331.
[4] J.G. Neels, P.A. Grimaldi, Physiological functions of peroxisome proliferator-activated receptor β, Physiol. Rev. 94 (2014) 795–858.
[5] B.P. Kota, T.H.W. Huang, B.D. Roufogalis, An overview on biological mechanisms of PPARs, Pharmacol. Res. 51 (2005) 85–94.

[6] O. Amber-Vitos, N. Chaturvedi, E. Nachliel, M. Gutman, Y. Tsfadia, The effect of regulating molecules on the structure of the PPAR-RXR complex, Biochim. Biophys. Acta Mol. Cell Biol. Lipids 1861 (2016) 1852–1863.
[7] F. Hong, P. Xu, Y. Zhai, The opportunities and challenges of peroxisome proliferator-activated receptors ligands in clinical drug discovery and development, Int. J. Mol. Sci. 19 (2018) 2189.
[8] T.M. Kadayat, A. Shrestha, Y.H. Jeon, H. An, J. Kim, S.J. Cho, J. Chin, Targeting peroxisome proliferator-activated receptor delta (PPARδ): a medicinal chemistry perspective, J. Med. Chem. 63 (2020) 10109–10134.
[9] M.H. Davidson, A. Armani, J.M. McKenney, T.A. Jacobson, Safety considerations with fibrate therapy, Am. J. Cardiol. 99 (2007). S3–S18.
[10] S. Yamashita, D. Masuda, Y. Matsuzawa, Pemafibrate, a new selective PPARα modulator: drug concept and its clinical applications for dyslipidemia and metabolic diseases, Curr. Atherosclerosis Rep. 22 (2020) 5.
[11] M. Bortolini, M.B. Wright, M. Bopst, B. Balas, Examining the safety of PPAR agonists - current trends and future prospects, Expet Opin. Drug Saf. 12 (2013) 65–79.
[12] A. Lavecchia, C. Cerchia, Selective PPARγ modulators for type 2 diabetes treatment: how far have we come and what does the future hold? *Future medicinal chemistry*, Future Science (2018) 703–705.
[13] C. Fiévet, J.C. Fruchart, B. Staels, PPARα and PPARγ dual agonists for the treatment of type 2 diabetes and the metabolic syndrome, Curr. Opin. Pharmacol. 6 (2006) 606–614.
[14] M. Heald, M.A. Cawthorne, Dual acting and pan-PPAR activators as potential anti-diabetic therapies, in: Diabetes-Perspectives in Drug Therapy, Springer, 2011, pp. 35–51.
[15] L. Piemontese, C. Cerchia, A. Laghezza, P. Ziccardi, S. Sblano, P. Tortorella, V. Iacobazzi, V. Infantino, P. Convertini, F. Dal Piaz, A. Lupo, V. Colantuoni, A. Lavecchia, F. Loiodice, New diphenylmethane derivatives as peroxisome proliferator-activated receptor alpha/gamma dual agonists endowed with anti-proliferative effects and mitochondrial activity, Eur. J. Med. Chem. 127 (2017) 379–397.
[16] L. Giampietro, A. Laghezza, C. Cerchia, R. Florio, L. Recinella, F. Capone, A. Ammazzalorso, I. Bruno, B. De Filippis, M. Fantacuzzi, C. Ferrante, C. MacCallini, P. Tortorella, F. Verginelli, L. Brunetti, A. Cama, R. Amoroso, F. Loiodice, A. Lavecchia, Novel phenyldiazenyl fibrate analogues as PPAR α/γ/δ pan-agonists for the amelioration of metabolic syndrome, ACS Med. Chem. Lett. 10 (2019) 545–551.
[17] U. Kaul, D. Parmar, K. Manjunath, M. Shah, K. Parmar, K.P. Patil, A. Jaiswal, New dual peroxisome proliferator activated receptor agonist—saroglitazar in diabetic dyslipidemia and non-alcoholic fatty liver disease: integrated analysis of the real world evidence, Cardiovasc. Diabetol. 18 (2019) 80.
[18] B. Boubia, O. Poupardin, M. Barth, J. Binet, P. Peralba, L. Mounier, E. Jacquier, E. Gauthier, V. Lepais, M. Chatar, Design, synthesis, and evaluation of a novel series of indole sulfonamide peroxisome proliferator activated receptor (PPAR) α/γ/δ triple activators: discovery of lanifibranor, a new antifibrotic clinical candidate, J. Med. Chem. 61 (2018) 2246–2265.
[19] X. Li, J. Yu, M. Wu, Q. Li, J. Liu, H. Zhang, X. Zhu, C. Li, J. Zhang, Z. Ning, Y. Ding, Pharmacokinetics and safety of chiglitazar, a peroxisome proliferator-activated receptor pan-agonist, in patients < 65 and ≥ 65 Years with type 2 diabetes, Clin. Pharmacol. Drug Dev. 10 (7) (2021) 789–796.
[20] D. Capelli, C. Cerchia, R. Montanari, F. Loiodice, P. Tortorella, A. Laghezza, L. Cervoni, G. Pochetti, A. Lavecchia, Structural basis for PPAR partial or full activation revealed by a novel ligand binding mode, Sci. Rep. 6 (2016) 1–12.
[21] D. Lagorce, O. Sperandio, J.B. Baell, M.A. Miteva, B.O. Villoutreix, FAF-Drugs3: a web server for compound property calculation and chemical library design, Nucleic Acids Res 43 (2015) W200–W207.
[22] C.A. Lipinski, F. Lombardo, B.W. Dominy, P.J. Feeney, Experimental and computational approaches to estimate solubility and permeability in drug discovery and development settings, Adv. Drug Deliv. Rev. 23 (1997) 3–25.
[23] A. Pinelli, C. Godio, A. Laghezza, N. Mitro, G. Fracchiolla, V. Tortorella, A. Lavecchia, E. Novellino, J.-C. Fruchart, B. Staels, Synthesis, biological evaluation, and molecular modeling investigation of new chiral fibrates with PPARα and PPARγ agonist activity, J. Med. Chem. 48 (2005) 5509–5519.
[24] J.R. Kramer, T.J. Deming, Glycopolypeptides with a redox-triggered helix-to-coil transition, J. Am. Chem. Soc. 134 (2012) 4112–4115.
[25] P. Gripon, S. Rumin, S. Urban, J. Le Seyec, D. Glaise, I. Cannie, C. Guyomard, J. Lucas, C. Trepo, C. Guguen-Guillouzo, Infection of a human hepatoma cell line by hepatitis B virus, Proc. Natl. Acad. Sci. U.S.A. 99 (2002) 15655–15660.
[26] S.N. Hart, Y. Li, K. Nakamoto, E.A. Subileau, D. Steen, X.B. Zhong, A comparison of whole genome gene expression profiles of HepaRG cells and HepG2 cells to primary human hepatocytes and human liver tissues, Drug Metab. Dispos. 38 (2010) 988–994.
[27] G.A. Nibourg, R.A. Chamuleau, T.V. van der Hoeven, M.A. Maas, A.F. Ruiter, W.H. Lamers, R.P. Oude Elferink, T.M. van Gulik, R. Hoekstra, Liver progenitor cell line HepaRG differentiated in a bioartificial liver effectively supplies liver support to rats with acute liver failure, PLoS One 7 (2012), e38778.
[28] A. Rogue, S. Anthérieu, A. Vluggens, T. Umbdenstock, N. Claude, C. de la Moureyre-Spire, R.J. Weaver, A. Guillouzo, PPAR agonists reduce steatosis in oleic acid-overloaded HepaRG cells, Toxicol. Appl. Pharmacol. 276 (2014) 73–81.
[29] C. Guzmán, M. Benet, S. Pisonero-Vaquero, M. Moya, M.V. García-Mediavilla, M.L. Martínez-Chantar, J. González-Gallego, J.V. Castell, S. Sánchez-Campos, R. Jover, The human liver fatty acid binding protein (FABP1) gene is activated by FOXA1 and PPARα; and repressed by C/EBPα: implications in FABP1 down-regulation in nonalcoholic fatty liver disease, Biochim. Biophys. Acta 1831 (2013) 803–818.
[30] Y. Zhao, M. Tran, L. Wang, D.J. Shin, J. Wu, PDK4-Deficiency reprograms intrahepatic glucose and lipid metabolism to facilitate liver regeneration in mice, Hepatol. Commun. 4 (2020) 504–517.
[31] M. Zhang, Y. Zhao, Z. Li, C. Wang, Pyruvate dehydrogenase kinase 4 mediates lipogenesis and contributes to the pathogenesis of nonalcoholic steatohepatitis, Biochem. Biophys. Res. Commun. 495 (2018) 582–586.
[32] Y. Zhang, T. Lei, J.F. Huang, S.B. Wang, L.L. Zhou, Z.Q. Yang, X.D. Chen, The link between fibroblast growth factor 21 and sterol regulatory element binding protein 1c during lipogenesis in hepatocytes, Mol. Cell. Endocrinol. 342 (2011) 41–47.
[33] M.J. Potthoff, T. Inagaki, S. Satapati, X. Ding, T. He, R. Goetz, M. Mohammadi, B.N. Finck, D.J. Mangelsdorf, S.A. Kliewer, S.C. Burgess, FGF21 induces PGC-1alpha and regulates carbohydrate and fatty acid metabolism during the adaptive starvation response, Proc. Natl. Acad. Sci. U.S.A. 106 (2009) 10853–10858.
[34] N. Itoh, Y. Nakayama, M. Konishi, Roles of FGFs as paracrine or endocrine signals in liver development, health, and disease, Front. Cell Dev. Biol. 4 (2016) 30.
[35] R. Hernandez, T. Teruel, M. Lorenzo, Rosiglitazone produces insulin sensitisation by increasing expression of the insulin receptor and its tyrosine kinase activity in brown adipocytes, Diabetologia 46 (2003) 1618–1628.
[36] T.A. Halgren, R.B. Murphy, R.A. Friesner, H.S. Beard, L.L. Frye, W.T. Pollard, J.L. Banks, Glide: a new approach for rapid, accurate docking and scoring. 2. Enrichment factors in database screening, J. Med. Chem. 47 (2004) 1750–1759.
[37] R.A. Friesner, J.L. Banks, R.B. Murphy, T.A. Halgren, J.J. Klicic, D.T. Mainz, M.P. Repasky, E.H. Knoll, M. Shelley, J.K. Perry, D.E. Shaw, P. Francis, P.S. Shenkin, Glide: a new approach for rapid, accurate docking and scoring. 1. Method and assessment of docking accuracy, J. Med. Chem. 47 (2004) 1739–1749.
[38] S. Kamata, T. Oyama, K. Saito, A. Honda, Y. Yamamoto, K. Suda, R. Ishikawa, T. Itoh, Y. Watanabe, T. Shibata, K. Uchida, M. Suematsu, I. Ishii, PPARα ligand-binding domain structures with endogenous fatty acids and fibrates, iScience 23 (2020).
[39] J.C. dos Santos, A. Bernardes, L. Giampietro, A. Ammazzalorso, B. De Filippis, R. Amoroso, I. Polikarpov, Different binding and recognition modes of GL479, a dual agonist of peroxisome proliferator-activated receptor α/γ, J. Struct. Biol. 191 (2015) 332–340.
[40] C.C. Wu, T.J. Baiga, M. Downes, J.J. La Clair, A.R. Atkins, S.B. Richard, W. Fan, T.A. Stockley-Noel, M.E. Bowman, J.P. Noel, R.M. Evans, Structural basis for specific ligation of the peroxisome proliferator-activated receptor δ, Proc. Natl. Acad. Sci. U. S. A 114 (2017) E2563–E2570.
[41] J.B. Bruning, M.J. Chalmers, S. Prasad, S.A. Busby, T.M. Kamenecka, Y. He, K.W. Nettles, P.R. Griffin, Partial agonists activate PPARγ using a helix 12 independent mechanism, Structure 15 (2007) 1258–1271.
[42] M.R. Berthold, N. Cebron, F. Dill, T.R. Gabriel, T. Kötter, T. Meinl, P. Ohl, K. Thiel, B. Wiswedel, KNIME-the konstanz information miner: version 2.0 and beyond, AcM SIGKDD Explor. Newsl. 11 (2009) 26–31.
[43] T. Sterling, J.J. Irwin, ZINC 15–ligand discovery for everyone, J. Chem. Inf. Model. 55 (2015) 2324–2337.
[44] J.B. Baell, G.A. Holloway, New substructure filters for removal of Pan assay interference compounds (PAINS) from screening libraries and for their exclusion in bioassays, J. Med. Chem. 53 (2010) 2719–2740.
[45] A. Pinelli, C. Godio, A. Laghezza, N. Mitro, G. Fracchiolla, V. Tortorella, A. Lavecchia, E. Novellino, J.-C. Fruchart, B. Staels, M. Crestani, F. Loiodice, Synthesis, biological evaluation, and molecular modeling investigation of new chiral fibrates with PPARalpha and PPARgamma agonist activity, J. Med. Chem. 48 (2005) 5509–5519.
[46] T. Hollon, F.K. Yoshimura, Variation in enzymatic transient gene expression assays, Anal. Biochem. 182 (1989) 411–418.
[47] V. Cerec, D. Glaise, D. Garnier, S. Morosan, B. Turlin, B. Drenou, P. Gripon, D. Kremsdorf, C. Guguen-Guillouzo, A. Corlu, Transdifferentiation of hepatocyte-like cells from the human hepatoma HepaRG cell line through bipotent progenitor, Hepatology 45 (2007) 957–967.